

Entanglement entropy of coherent intertwiner in loop quantum gravity

Gaoping Long^{1,*}, Qian Chen^{2,†} and Jinsong Yang^{3,‡}

¹*College of Physics and Optoelectronic Engineering, Jinan University, Guangzhou, 510632, Guangdong, China*

²*Université de Lyon, Inria, ENS Lyon, UCBL, LIP, F-69342, Lyon Cedex 07, France*

³*School of Physics, Guizhou University, Guiyang 550025, China*



(Received 26 March 2024; accepted 26 July 2024; published 5 September 2024)

In this paper, we carry out the entanglement calculations on the coherent intertwiners. We first consider the entanglement introduced by the group averaging of the tensor-product-type intertwiner on a 4-valents vertex. Then, we calculate explicitly the entanglement carried by the gauge-invariant coherent intertwiner with four legs. Our numerical results show that the entanglement can be controlled by the local semiclassical geometry described by the coherent intertwiner. We also extend our analytical calculation to the coherent intertwiners with an arbitrary number of legs. Especially, we apply the previous results to the entanglement of the spin-network state labeled by coherent intertwiners, with the network puncturing a boundary by its vertices. We show that the entanglement of such spin-network state is not only determined by the area of the boundary but also carries a quantum correction controlled by the semiclassical geometry associated to the vertices puncturing the boundary.

DOI: [10.1103/PhysRevD.110.064017](https://doi.org/10.1103/PhysRevD.110.064017)

I. INTRODUCTION

Loop quantum gravity (LQG) provides a background-independent and nonperturbative quantum theory of General Relativity (GR) [1–6]. Specifically, LQG defines the quantum states of spatial intrinsic and extrinsic geometry as spin networks. The quantum geometry carried by spin networks can be understood as the quantization of discrete twisted geometries [7–12], while the information of quantum geometry encoded in spin-network states can be extracted by the geometric operators in LQG [13–17]. The quantum evolution of spin networks is governed by the Hamiltonian operator in canonical formulation [18–21] or described by the path-integral formulation [22–26]. Besides, the semiclassical geometries at the discrete stage can be given by the expectation values of the geometric operators based on the coherent states, which are constructed by specific superposition of intertwiners and spin networks [27–34].

As a quantum gravity theory, LQG also provides us a platform to study the black hole thermodynamics in a fundamental perspective. More explicitly, the Bekenstein-Hawking entropy, which is supposed to originate from a quantum theory of gravity, is first derived in classical GR coupled to quantum matter field. It is natural to expect that the Bekenstein-Hawking entropy can be derived from an

ab initio computation of the entropy based on the microstates in a specific quantum gravity theory. In fact, in the LQG framework, the nonperturbative computation of black hole entropy has been performed based on the quantum isolated horizons described by quantum Chern-Simons theory coupled to bulk LQG in several works [35–50], which lead to specific corrections to the Bekenstein-Hawking entropy. Another strong candidate of the source of black hole entropy is the entanglement entropy between the quantum system inside and outside the black hole horizon [51–55]. This approach is based on the observation that the entanglement between quantum systems inside and outside the horizon is caused by the fact that the globally pure state becomes mixed since the horizon hide the degrees of freedom of the interior of the black hole [51,52]. Specifically, the entanglement in LQG is computed for black hole coherent states in spherically symmetric spacetime with apparent horizons in Ref. [53], and it is computed for the spin-network basis without assumption of symmetry or of specific boundary conditions at the horizon in Ref. [51]. It has been argued that the entropy computed in the isolated horizon framework of LQG is closely related to the entanglement entropy of the gravitational field in several previous works [52,56].

Particularly, it has been shown that the entanglement carried by the spin-network basis state is the composition of the entanglement carried by the intertwiners on the boundary [51]. However, the previous computation merely involves the case that only edges of the network puncture the boundary, and the computation results show that the

*Contact author: 201731140005@mail.bnu.edu.cn

†Contact author: chenqian.phys@gmail.com

‡Contact author: jsyang@gzu.edu.cn

edge puncturing the boundary with spin j contributes $\ln(2j+1)$ to the total entanglement entropy. Moreover, it is pointed out that the entanglement carried by the superposed intertwiners is much more than a term given by $\ln(2j+1)$ [57]. Thus, the computation of the entanglement for spin-network states labeled by superposed intertwiners is a valuable topic in LQG. A typical method to introduce the superposition of intertwiners is imposing the gauge averaging over the product state, with this superposition reflecting the requirement of the gauge invariance. Besides, the gauge averaging over some coherent states gives the gauge-invariant coherent intertwiner, which provides a semiclassical description of the discrete spatial geometry, i.e., minimizes the uncertainty of the expectation values of the area and face-angle operators [58–60]. In this paper, we will focus on the mechanism of group averaging to the entanglement, specifically, of coherent intertwiners, and then analyze the entanglement entropy of spin network labeled by coherent intertwiners. Our results show that the entanglement of coherent intertwiner can be controlled by the semiclassical geometry associated to the vertex, i.e., the expectation values of area and angle operators; moreover, for the spin network puncturing a boundary by its vertices labeled by coherent intertwiners, we show that the entanglement entropy of such a spin network is not only determined by the area of the boundary but also carries a quantum correction controlled by the semiclassical geometry associated to the vertices on the boundary.

This paper is organized as follows. After the basic structure of spin-network state and intertwiner in LQG is introduced in Sec. II, the entanglements on the kinds of spin-network states and intertwiners are calculated. Specifically, in Sec. III A, we generalize the relation between boundary entanglement and intertwiner entanglement to the case in which the internal edge carries spin superposition. Then, we calculate the entanglement introduced by the group averaging of the tensor-product type intertwiner with four legs by numerical method in Sec. III B. Further, in Sec. III C 1, this calculation is extended to the gauge-invariant coherent intertwiner with four legs. Moreover, in Sec. III C 2, we also carry out some key analytical calculations for the entanglement on the coherent intertwiners with arbitrary number of legs. Besides, we apply the results in previous sections to discuss the entanglement of spin-network states in Sec. IV. Finally, in Sec. V, we finish with conclusion and discussion for our results.

II. SPIN-NETWORK STATE AND INTERTWINER IN LOOP QUANTUM GRAVITY

The Hilbert space \mathcal{H}_Γ for quantum geometry on a closed oriented graph Γ embedded in a three-dimensional manifold is composed by the square integrable functions on $SU(2)$ associated to each edge $e \in \Gamma$, which are invariant under the $SU(2)$ action at every vertex $v \in \Gamma$. Specifically, a

square integrable function on Γ takes the formulation

$$\Psi_\Gamma = \Psi_\Gamma(\{h_e\}_{e \in \Gamma}). \quad (1)$$

The $SU(2)$ gauge invariance at the vertex of Ψ_Γ reads

$$\Psi_\Gamma(\{h_e\}_{e \in \Gamma}) = \Psi_\Gamma(\{g_{s(e)} h_e g_{t(e)}^{-1}\}_{e \in \Gamma}), \quad (2)$$

where $\{g_v | v \in \Gamma\}$ are given at each vertex $v \in \Gamma$ respectively, $s(e)$ represents the source vertex of e , and $t(e)$ represents the target vertex of e . The spin-network states provide a basis of space \mathcal{H}_Γ . Specifically, a (nonsuperposed) spin-network basis state on Γ is given by labeling a spin $j_e \in \frac{\mathbb{N}}{2}$ on each edge $e \in \Gamma$ and an intertwiner \mathcal{I}_v on each vertex $v \in \Gamma$, which reads [2]

$$\Psi_{\Gamma, \{j_e, \mathcal{I}_v\}} = \text{tr} \left(\bigotimes_{e \in \Gamma} \pi_{j_e}(h_e) \bigotimes_{v \in \Gamma} \mathcal{I}_v \right), \quad (3)$$

where $\pi_{j_e}(h_e)$ is the representation matrix of $h_e \in SU(2)$ in the representation space V^{j_e} of $SU(2)$ labeled by spin j_e , and $\mathcal{I}_v \in \bigotimes_{e|t(e)=v} V^{j_e} \otimes \bigotimes_{e|s(e)=v} \bar{V}^{j_e}$. Especially, the spin-network state $\Psi_{\Gamma, \{j_e, \mathcal{I}_v\}}$ is gauge invariant if and only if each $v \in \Gamma$ is labeled by a gauge-invariant intertwiner. Another basis of space \mathcal{H}_Γ is given by the coherent state of spin networks. The coherent state of spin network is the superposition of spin networks, which reads [27]

$$\Psi_{\Gamma, G}^t(h) = \prod_{e \in \Gamma} \Psi_{G_e}^t(h_e) \quad (4)$$

with

$$\Psi_{G_e}^t(h_e) := \sum_{j_e \in \frac{\mathbb{N}}{2}} (2j_e + 1) e^{-t j_e (j_e + 1)/2} \chi_{j_e}(h_e G_e^{-1}), \quad (5)$$

where $G = \{G_e\}_{e \in \Gamma}$, $h = \{h_e\}_{e \in \Gamma}$, χ_j is the $SU(2)$ character with spin j , and $t \propto \kappa \hbar$ is a semiclassicality parameter. As a function of the holonomies h_e , the coherent state is labeled by G_e , with $G_e \in T^*SU(2) \cong SL(2, \mathbb{C})$ being the complex coordinates of the discrete holonomy-flux phase space of LQG. The gauge-invariant coherent state of the spin network is labeled by the gauge equivalent class of $G_e \sim G_e^g := g_{s(e)}^{-1} G_e g_{t(e)}$ for all $e \in \Gamma$, where $g = \{g_v \in SU(2) | v \in \Gamma\}$. Equivalently, the gauge-invariant coherent state of the spin network is also labeled by the gauge-invariant intertwiners at each $v \in \Gamma$. Let us give an explicit introduction of gauge-invariant intertwiner as follows.

The gauge-invariant intertwiner \mathcal{I}_v at vertex v is a $SU(2)$ -invariant state in the tensor product space of all the spins associated to the edges linked to v ,

$$\mathcal{I}_v \in \mathcal{H}_v^{\{j_e\}} := \text{Inv}_{SU(2)} \left[\bigotimes_{e|t(e)=v} V^{j_e} \otimes \bigotimes_{e|s(e)=v} \bar{V}^{j_e} \right], \quad (6)$$

where \bar{V}^j is the dual space of V^j . The space V^j has dimension $d_j = (2j+1)$ and the orthonormal basis $\{|j, m\rangle | -j \leq m \leq j\}$, which diagonalize the $su(2)$ Casimir $\vec{J}^2 := J_x J_x + J_y J_y + J_z J_z$ and the generator J_3 as

$$\vec{J}^2 |j, m\rangle = j(j+1) |j, m\rangle, \quad J_z |j, m\rangle = m |j, m\rangle. \quad (7)$$

An orthonormal basis of the intertwiner space $\mathcal{H}_v^{\{j_e\}}$ is established by the recoupling scheme, which reads

$$\{\mathcal{I}_{v, \{j_i\}}^{\{j_e\}} = \mathcal{I}_{v, \{j_{i_1}, j_{i_2}, \dots, j_{i_{N_v-3}}\}}^{\{j_e\}} \in \mathcal{H}_v^{\{j_e\}}, \quad (8)$$

where N_v is the number of the edges which link to v , and $\{j_{i_1}, j_{i_2}, \dots, j_{i_{N_v-3}}\}$ labeling the internal edges in the recoupling scheme, which satisfies

$$\begin{aligned} |j_{e_1} - j_{e_2}| \leq j_{i_1} \leq j_{e_1} + j_{e_2}, \quad |j_{i_1} - j_{e_3}| \leq j_{i_2} \leq j_{i_1} + j_{e_3}, \\ \dots, |j_{i_{N_v-5}} - j_{e_{N_v-3}}| \leq j_{i_{N_v-4}} \leq j_{i_{N_v-5}} + j_{e_{N_v-3}}, \\ |j_{i_{N_v-4}} - j_{e_{N_v-2}}| \leq j_{i_{N_v-3}} \leq j_{i_{N_v-4}} + j_{e_{N_v-2}}, \\ |j_{e_{N_v-1}} - j_{e_{N_v}}| \leq j_{i_{N_v-3}} \leq j_{e_{N_v-1}} + j_{e_{N_v}}. \end{aligned} \quad (9)$$

Another basis of the intertwiner space $\mathcal{H}_v^{\{j_e\}}$ is the so-called coherent intertwiner basis [58,61], which is established based on the $SU(2)$ coherent state. A $SU(2)$ coherent state $|j, \hat{n}\rangle$ is defined via rotating the highest weight state $|j, j\rangle$ by $g(\hat{n}) \in SU(2)$, namely [62],

$$|j, \hat{n}\rangle = g(\hat{n}) |j, j\rangle, \quad (10)$$

where \hat{n} is a unit vector, and $g(\hat{n}) \in SU(2)$ satisfies $\hat{n} = g(\hat{n}) \hat{z}$ with the north pole vector $\hat{z} = (0, 0, 1) \in \mathbb{S}^2$. The $SU(2)$ coherent state $|j, \hat{n}\rangle$ can be decomposed by the orthonormal basis $\{|j, m\rangle\}$ as [62]

$$|j, \hat{n}\rangle = \sum_{m=-j}^j c_{j,m}(\hat{n}) |j, m\rangle, \quad (11)$$

where

$$\begin{aligned} c_{j,m}(\hat{n}) = & \left(\frac{(2j)!}{(j+m)!(j-m)!} \right)^{\frac{1}{2}} \left(-\sin \frac{\pi - \theta}{2} \right)^{j+m} \\ & \times \left(\cos \frac{\pi - \theta}{2} \right)^{j-m} \exp(-i(j+m)(\varphi + \pi)) \end{aligned} \quad (12)$$

with $\hat{n} = (\sin \theta \cos \varphi, \sin \theta \sin \varphi, \cos \theta)$. Moreover, the $SU(2)$ coherent states $|j, \hat{n}\rangle$ provide a overcomplete basis of the space V^j as

$$\mathbb{I}_{V^j} = (2j+1) \int_{\mathbb{S}^2} dn |j, \hat{n}\rangle \langle j, \hat{n}|, \quad (13)$$

where \mathbb{I}_{V^j} is the identity of V^j and dn is the normalized measure on the 2-sphere \mathbb{S}^2 . Now, the coherent intertwiner basis of $\mathcal{H}_v^{\{j_e\}}$ can be given as

$$\mathbb{I}_{\mathcal{H}_v^{\{j_e\}}} = \int_{\mathcal{S}_v^{\{j_e\}}} d\sigma_v^{\{j_e\}} |\mathcal{I}_{v, \{j_e\}}^{\{\hat{n}_e\}}\rangle \langle \mathcal{I}_{v, \{j_e\}}^{\{\hat{n}_e\}}|, \quad (14)$$

where $\{\hat{n}_e\} \equiv (\hat{n}_{e_1}, \dots, \hat{n}_{e_{N_v}})$, $\mathcal{S}_v^{\{j_e\}} := \{(\hat{n}_{e_1}, \dots, \hat{n}_{e_{N_v}}) \in \times_{I=1}^{N_v} \mathbb{S}_I^2 | \sum_{e|t(e)=v} j_e \hat{n}_e - \sum_{e|s(e)=v} j_e \hat{n}_e = 0\} / SU(2)$, $d\sigma_v^{\{j_e\}}$ is an invariant measure on $\mathcal{S}_v^{\{j_e\}}$, and the coherent intertwiner $|\mathcal{I}_{v, \{j_e\}}^{\{\hat{n}_e\}}\rangle$ is given by the following $SU(2)$ -group averaging:

$$|\mathcal{I}_{v, \{j_e\}}^{\{\hat{n}_e\}}\rangle := \int_{SU(2)} dg \bigotimes_{e|t(e)=v} g |j_e, \hat{n}_e\rangle \bigotimes_{e|s(e)=v} \langle j_e, \hat{n}_e | g^{-1}. \quad (15)$$

To simplify our notations and distinguish the labels of the ingoing and outgoing edges, we use j, \hat{n} to label the ingoing edges and $\tilde{j}, \hat{\tilde{n}}$ to the outgoing edges. Then, the coherent intertwiner can be reformulated as

$$|\mathcal{I}_{v, \{j, \tilde{j}\}}^{\{\hat{n}, \hat{\tilde{n}}\}}\rangle := \int_{SU(2)} dg \bigotimes_{I=1}^P g |j_I, \hat{n}_I\rangle \bigotimes_{J=1}^Q \langle \tilde{j}_J, \hat{\tilde{n}}_J | g^{-1}, \quad (16)$$

where P is the number of the edges ended at v and Q is the number of the edges started at v .

The $SU(2)$ coherent states are said to be semiclassical states due to the property that they minimize the Heisenberg uncertainty relation [58,59,62]. A coherent spin state $|j, \hat{n}\rangle$ picks the unit vector \hat{n} by \vec{J} as $\hat{n} = \lim_{j \rightarrow \infty} \frac{(j, \hat{n} | \vec{J} | j, \hat{n})}{j}$. In the framework of LQG, each vertex $v \in \Gamma$ is dual to a polyhedron, and the edges attached to the v are dual to the faces of the polyhedron [60,63]. The area and the normal vector of the face are characterized by j and \hat{n} from $|j, \hat{n}\rangle$, respectively. These pair data $\{(j, \hat{n})\}$ indeed provide a semiclassical but gauge-variant picture. The gauge invariance is fulfilled via $SU(2)$ -group averaging over the tensoring spin states $\bigotimes_{e|t(e)=v} |j_e, \hat{n}_e\rangle \bigotimes_{e|s(e)=v} \langle j_e, \hat{n}_e |$ with $\{\hat{n}_e\} \in \mathcal{S}_v^{\{j_e\}}$, defining a gauge-invariant coherent intertwiner. Although the information about the direction of each unit vector \hat{n}_e loses due to the $SU(2)$ -group averaging, the relative angles among these unit vectors survive. Hence, a polyhedron in discrete geometry can be built from gauge-invariant coherent intertwiners in a relational picture [58,60,63]: for a v around by N_v faces, the $\{j_e\}$ determines N_v areas, and $\{\hat{n}_e\} \in \mathcal{S}_v^{\{j_e\}}$ determines $2N_v - 6$ relative angles.

III. DENSITY MATRIX AND ENTANGLEMENT ENTROPY OF COHERENT INTERTWINER

A. Boundary and intertwiner entanglement entropies

Consider a two-vertices graph Γ as illustrated in Fig. 1: one vertex v_1 is attached by $P + 1$ edges, and another vertex v_2 is attached by $Q + 1$ edges; meanwhile, v_1 and v_2 are connected by edge e . For the sake of simplifying the notations, we reorient all of the edges to ensure that e is outgoing at v_1 and ingoing at v_2 with other edges being ingoing at v_1 and outgoing at v_2 without losing generality. Then, the boundary Hilbert space for this system is defined as

$$\mathcal{H}_{\partial\Gamma} := \bigotimes_{I=1}^P V^I \otimes \bigotimes_{J=1}^Q \bar{V}^J. \quad (17)$$

That is, excluding the Hilbert space associated with the internal edge e whose two ends are contained in the graph. The apparent bipartition on the boundary Hilbert space is given by

$$\begin{aligned} \mathcal{H}_{\partial\Gamma} &= \mathcal{H}_{v_1}^\partial \otimes \mathcal{H}_{v_2}^\partial, \quad \text{where } \mathcal{H}_{v_1}^\partial := \bigotimes_{I=1}^P V^I, \quad \text{and} \\ \mathcal{H}_{v_2}^\partial &:= \bigotimes_{J=1}^Q \bar{V}^J. \end{aligned} \quad (18)$$

On the other hand, the intertwiner Hilbert space on graph Γ is defined as

$$\begin{aligned} \mathcal{H}_\Gamma &:= \mathcal{H}_{v_1} \otimes \mathcal{H}_{v_2}, \quad \text{where } \mathcal{H}_{v_1} := \text{Inv} \left(\bigotimes_{I=1}^P V_I \otimes \bar{V}_e \right) \quad \text{and} \\ \mathcal{H}_{v_2} &:= \text{Inv} \left(V^e \otimes \bigotimes_{J=1}^Q \bar{V}_J \right). \end{aligned} \quad (19)$$

The gluing map [57] provides a correspondence between the boundary state $|\psi_\Gamma\rangle_\partial \in \mathcal{H}_{\partial\Gamma}$ and the intertwiner state $|\psi_\Gamma\rangle \in \mathcal{H}_\Gamma$. Intuitively, the gluing map glues the boundary edges together along the internal edges. Let us illustrate the gluing map as follows. Assume that the internal edge e that links v_1 and v_2 carries a fixed j . Then, the spin-network state is written as

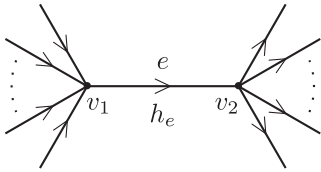


FIG. 1. The 2-vertex graph Γ . The holonomy h_e along the edge e that connects v_1 and v_2 contributes nothing to the entanglement entropy.

$$\begin{aligned} |\Psi_\Gamma^j\rangle &= \sum_{\{j_I, \tilde{j}_I, j_I, \tilde{j}_I\}} \mathcal{C}_{\mathcal{I}_{v_1, \{j_I\}}^{(j_I), j} \mathcal{I}_{v_2, \{\tilde{j}_I\}}^{(j_I), j}} \\ &\times \underbrace{\left(\sum_{m, \{m_I\}} \mathcal{I}_{m_1 \dots m_P m}^{j_1 \dots j_P j, \{j_I\}} \bigotimes_{I=1}^P |j_I, m_I\rangle \langle j, m| \right)}_{=|\mathcal{I}_{v_1, \{j_I\}}^{(j_I), j}\rangle} \\ &\otimes \underbrace{\left(\sum_{n, \{\tilde{m}_J\}} |j, n\rangle \bigotimes_{J=1}^Q \langle \tilde{j}_J, \tilde{m}_J | \mathcal{I}_{n \tilde{m}_1 \dots \tilde{m}_Q}^{j \tilde{j}_1 \dots \tilde{j}_Q, \{\tilde{j}_J\}} \right)}_{=|\mathcal{I}_{v_2, \{\tilde{j}_J\}}^{(j_I), j}\rangle}. \end{aligned} \quad (20)$$

Let us explain the notations in this equation: (i) j_I, \tilde{j}_I label the boundary edges of Γ in left and right side, respectively, and j_I, \tilde{j}_I represent the recoupling spins for the coherent intertwiner basis $\mathcal{I}_{v_1, \{j_I\}}^{(j_I), j}$ and $\mathcal{I}_{v_2, \{\tilde{j}_I\}}^{(j_I), j}$, respectively. (ii) The coefficients $\mathcal{I}_{m_1 \dots m_P m}^{j_1 \dots j_P j, \{j_I\}}$ as well as $\mathcal{I}_{n \tilde{m}_1 \dots \tilde{m}_Q}^{j \tilde{j}_1 \dots \tilde{j}_Q, \{\tilde{j}_I\}}$ are responsible for the gauge invariances of $\mathcal{I}_{v_1, \{j_I\}}^{(j_I), j}$ and $\mathcal{I}_{v_2, \{\tilde{j}_I\}}^{(j_I), j}$, respectively, which can be constructed by concatenating Clebsch-Gordan coefficients. (iii) The coefficients $\mathcal{C}_{\mathcal{I}_{v_1, \{j_I\}}^{(j_I), j} \mathcal{I}_{v_2, \{\tilde{j}_I\}}^{(j_I), j}}$ encode the correlation between intertwiners living at v_1 and v_2 . On the other hand, the boundary state associated with the spin network is written as

$$\begin{aligned} |\Psi_\Gamma^j\rangle_\partial &= \sum_{\{j_I, \tilde{j}_I, j_I, \tilde{j}_I\}} \sqrt{2j+1} \mathcal{C}_{\mathcal{I}_{v_1, \{j_I\}}^{(j_I), j} \mathcal{I}_{v_2, \{\tilde{j}_I\}}^{(j_I), j}} \cdot \sum_{m, n, \{m_I, \tilde{m}_J\}} \mathcal{I}_{m_1 \dots m_P m}^{j_1 \dots j_P j, \{j_I\}} \\ &\bigotimes_{I=1}^P |j_I, m_I\rangle D_{mn}^j(h_e) \bigotimes_{J=1}^Q \langle \tilde{j}_J, \tilde{m}_J | \mathcal{I}_{n \tilde{m}_1 \dots \tilde{m}_Q}^{j \tilde{j}_1 \dots \tilde{j}_Q, \{\tilde{j}_I\}}, \end{aligned} \quad (21)$$

where $D_{mn}^j(h_e) := \langle j, m | h_e | j, n \rangle$. The gluing map is then viewed as sending $|\Psi_\Gamma^j\rangle$ to $|\Psi_\Gamma^j\rangle_\partial$, via sandwiching holonomy that associates the edge to be glued. This gluing map can also be established without the holonomy insertion [i.e., setting $h_e = \text{identity}$ in Eq. (21)], which leads to

$$\begin{aligned} |\check{\Psi}_\Gamma^j\rangle_\partial &= \sum_{\{j_I, \tilde{j}_I, j_I, \tilde{j}_I\}} \sqrt{2j+1} \mathcal{C}_{\mathcal{I}_{v_1, \{j_I\}}^{(j_I), j} \mathcal{I}_{v_2, \{\tilde{j}_I\}}^{(j_I), j}} \sum_{m, \{m_I, \tilde{m}_J\}} \mathcal{I}_{m_1 \dots m_P m}^{j_1 \dots j_P j, \{j_I\}} \\ &\bigotimes_{I=1}^P |j_I, m_I\rangle \bigotimes_{J=1}^Q \langle \tilde{j}_J, \tilde{m}_J | \mathcal{I}_{m \tilde{m}_1 \dots \tilde{m}_Q}^{j \tilde{j}_1 \dots \tilde{j}_Q, \{\tilde{j}_I\}}. \end{aligned} \quad (22)$$

Now, we look at the entanglement carried by these states. The intertwiner entanglement entropy $E(v_1|v_2)$ with respect to $\mathcal{H}_\Gamma = \mathcal{H}_{v_1} \otimes \mathcal{H}_{v_2}$ is given by the von Neumann entropy from below reduced density matrix

$$\rho_{v_1}^j := \text{Tr}_{\mathcal{H}_{v_2}} |\Psi_\Gamma^j\rangle \langle \Psi_\Gamma^j| \quad (23)$$

$$\begin{aligned} &= \sum_{\{j_I, \tilde{j}_I, j_I, \tilde{j}_I\}} \sum_{\{\tilde{j}_I, \tilde{j}_I\}} \mathcal{C}_{\mathcal{I}_{v_1, \{j_I\}}^{(j_I), j} \mathcal{I}_{v_2, \{\tilde{j}_I\}}^{(j_I), j}} \overline{\mathcal{C}_{\mathcal{I}_{v_1, \{j_I\}}^{(j_I), j} \mathcal{I}_{v_2, \{\tilde{j}_I\}}^{(j_I), j}}} |\mathcal{I}_{v_1, \{j_I\}}^{(j_I), j}\rangle \langle \mathcal{I}_{v_1, \{j_I\}}^{(j_I), j}|. \end{aligned} \quad (24)$$

On the other hand, the boundary entanglement entropy $E(v_1^\partial|v_2^\partial)$ with respect to $\mathcal{H}_{\partial\Gamma} = \mathcal{H}_{v_1}^\partial \otimes \mathcal{H}_{v_2}^\partial$ is given by the von Neumann entropy from the reduced density matrix

$$\begin{aligned} \rho_{v_1}^{\partial,j} &:= \text{Tr}_{\mathcal{H}_{v_2}^\partial} |\Psi_\Gamma^j\rangle\langle\Psi_\Gamma^j|_\partial = \text{Tr}_{\mathcal{H}_{v_2}^\partial} |\check{\Psi}_\Gamma^j\rangle\langle\check{\Psi}_\Gamma^j|_\partial \\ &= \sum_{\{j_I, j'_I, j_I, j'_I\}} \sum_{\{\tilde{j}_I, \tilde{j}_I\}} \mathcal{C}_{\mathcal{I}_{v_1, \{j_I\}}^{(j_I), j} \mathcal{I}_{v_2, \{\tilde{j}_I\}}^{(\tilde{j}_I), j}} \overline{\mathcal{C}_{\mathcal{I}_{v_1, \{j'_I\}}^{(j'_I), j} \mathcal{I}_{v_2, \{\tilde{j}_I\}}^{(\tilde{j}_I), j}}} \\ &\quad \times \sum_{m, \{m_I, m'_I\}} \mathcal{I}_{m_1, \dots, m_p, m}^{j_1, \dots, j_p, j, \{j_I\}} \overline{\mathcal{I}_{m'_1, \dots, m'_p, m}^{j'_1, \dots, j'_p, j, \{j'_I\}}} \bigotimes_{I=1}^P |j_I, m_I\rangle\langle j'_I, m'_I| \\ &= \sum_{\{j_I, j'_I, j_I, j'_I\}} \sum_{\{\tilde{j}_I, \tilde{j}_I\}} \mathcal{C}_{\mathcal{I}_{v_1, \{j_I\}}^{(j_I), j} \mathcal{I}_{v_2, \{\tilde{j}_I\}}^{(\tilde{j}_I), j}} \overline{\mathcal{C}_{\mathcal{I}_{v_1, \{j'_I\}}^{(j'_I), j} \mathcal{I}_{v_2, \{\tilde{j}_I\}}^{(\tilde{j}_I), j}}} \\ &\quad \times \sum_m \langle j, m | \mathcal{I}_{v_1, \{j_I\}}^{\{j_I\}, j} \rangle \langle \mathcal{I}_{v_1, \{j'_I\}}^{\{j'_I\}, j} | j, m \rangle, \end{aligned} \quad (26)$$

where $\mathcal{H}_{v_2}^\partial = \bigotimes_{J=1}^Q \bar{V}_J$ is the boundary-edge state space attached to the vertex v_2 , and the following orthogonality is used:

$$\sum_{\{m_I\}_{I=1}^N} \mathcal{I}_{m_1, \dots, m_N, m}^{j_1, \dots, j_N, j, \{j_I\}} \overline{\mathcal{I}_{m'_1, \dots, m'_N, m}^{j'_1, \dots, j'_N, j, \{j'_I\}}} = \frac{1}{2j+1} \delta_{jj'} \delta_{mm'} \delta_{\{j_I\}\{j'_I\}}. \quad (27)$$

Indeed, one can verify the normalization $\text{Tr}_{\mathcal{H}_{v_1}^\partial} \rho_{v_1}^{\partial,j} = 1$. Note that the relation between the two density matrices can be given by

$$\rho_{v_1}^{\partial,j} = \text{Tr}_{V_e} \rho_{v_1}^j \quad (28)$$

with $V_e = V^j$. That is to say, the reduced density matrix $\rho_{v_1}^{\partial,j}$ of the half-cut boundary can be understood as tracing the reduced density matrix $\rho_{v_1}^j$ of the half-cut graph over the recoupled Hilbert space (here, it is V^j associative with the spin j along the internal edge e). Then, following Ref. [57], one can show a simple relation between the entanglement entropy of $\mathcal{H}_{\partial\Gamma} = \mathcal{H}_{v_1}^\partial \otimes \mathcal{H}_{v_2}^\partial$ and of $\mathcal{H}_\Gamma = \mathcal{H}_{v_1} \otimes \mathcal{H}_{v_2}$.

Theorem 1. In the cases in which the spin along the internal edge is fixed at j , the following relation between entanglement entropies holds [57]:

$$E_j(v_1^\partial|v_2^\partial) = E_j(v_1|v_2) + \ln(2j+1), \quad (29)$$

where $E_j(v_1^\partial|v_2^\partial) := -\text{Tr}(\rho_{v_1}^{\partial,j} \ln \rho_{v_1}^{\partial,j})$ and $E_j(v_1|v_2) := -\text{Tr}(\rho_{v_1}^j \ln \rho_{v_1}^j)$.

Notice that Theorem 1 only involves the case in which the internal edge has a fixed spin j . Now, we would like to generalize the relation Eq. (29) to the cases that the internal edge e carries spin superposition. Let us consider the state

$$\begin{aligned} |\Psi_\Gamma\rangle &= \sum_j \alpha_j |\Psi_\Gamma^j\rangle = \sum_j \sum_{\{j_I, \tilde{j}_I, j_I, \tilde{j}_I\}} \alpha_j \mathcal{C}_{\mathcal{I}_{v_1, \{j_I\}}^{(j_I), j} \mathcal{I}_{v_2, \{\tilde{j}_I\}}^{(\tilde{j}_I), j}} |\mathcal{I}_{v_1, \{j_I\}}^{\{j_I\}, j}\rangle \\ &\quad \otimes |\mathcal{I}_{v_2, \{\tilde{j}_I\}}^{\{\tilde{j}_I\}, j}\rangle, \end{aligned} \quad (30)$$

the gluing state with holonomy insertion

$$\begin{aligned} |\Psi_\Gamma\rangle_\partial &= \sum_j \alpha_j \sum_{\{j_I, \tilde{j}_I, j_I, \tilde{j}_I\}} \sqrt{2j+1} \mathcal{C}_{\mathcal{I}_{v_1, \{j_I\}}^{(j_I), j} \mathcal{I}_{v_2, \{\tilde{j}_I\}}^{(\tilde{j}_I), j}} \\ &\quad \cdot \sum_{m, n, \{m_I, \tilde{m}_I\}} \mathcal{I}_{m_1, \dots, m_p, m}^{j_1, \dots, j_p, j, \{j_I\}} \bigotimes_{I=1}^P |j_I, m_I\rangle D_{mn}^j(h_e) \\ &\quad \bigotimes_{J=1}^Q \langle \tilde{j}_J, \tilde{m}_J | \mathcal{I}_{n\tilde{m}_1, \dots, \tilde{m}_Q}^{j\tilde{j}_1, \dots, \tilde{j}_Q, \{\tilde{j}_I\}} \rangle, \end{aligned} \quad (31)$$

and the gluing state without holonomy insertion

$$\begin{aligned} |\check{\Psi}_\Gamma\rangle_\partial &= \sum_j \alpha_j \sum_{\{j_I, \tilde{j}_I, j_I, \tilde{j}_I\}} \sqrt{2j+1} \mathcal{C}_{\mathcal{I}_{v_1, \{j_I\}}^{(j_I), j} \mathcal{I}_{v_2, \{\tilde{j}_I\}}^{(\tilde{j}_I), j}} \\ &\quad \times \sum_{m, \{m_I, \tilde{m}_I\}} \mathcal{I}_{m_1, \dots, m_p, m}^{j_1, \dots, j_p, j, \{j_I\}} \bigotimes_{I=1}^P |j_I, m_I\rangle \\ &\quad \bigotimes_{J=1}^Q \langle \tilde{j}_J, \tilde{m}_J | \mathcal{I}_{m\tilde{m}_1, \dots, \tilde{m}_Q}^{j\tilde{j}_1, \dots, \tilde{j}_Q, \{\tilde{j}_I\}} \rangle. \end{aligned} \quad (32)$$

Again, the reduced density matrices are obtained via partial tracing in $\mathcal{H}_{v_2}^\partial$ and \mathcal{H}_{v_2} , respectively, which gives

$$\tilde{\rho}_{v_1}^\partial := \text{Tr}_{\mathcal{H}_{v_2}^\partial} |\Psi_\Gamma\rangle\langle\Psi_\Gamma|_\partial = \text{Tr}_{\mathcal{H}_{v_2}^\partial} |\check{\Psi}_\Gamma\rangle\langle\check{\Psi}_\Gamma|_\partial, \quad (33)$$

and

$$\tilde{\rho}_{v_1} := \text{Tr}_{\mathcal{H}_{v_2}} |\Psi_\Gamma\rangle\langle\Psi_\Gamma|. \quad (34)$$

Similarly, the generalized relation between $\tilde{\rho}_{v_1}^\partial$ and $\tilde{\rho}_{v_1}$ holds by taking superposition of j into account, which reads

$$\tilde{\rho}_{v_1}^\partial = \text{Tr}_{V_e} \tilde{\rho}_{v_1}, \quad (35)$$

where $V_e = \bigoplus_j V^j$ and $\tilde{\rho}_{v_1} = \bigoplus_j \tilde{\rho}_j \rho_{v_1}^j$ with $\tilde{\rho}_j \equiv \alpha_j \bar{\alpha}_j$. Then, the relation between intertwiners and boundary entanglements leads the following theorem.

Theorem 2. In the cases in which the spin along the internal edge is superposed, say, the intertwiner state is given by $|\Psi_\Gamma\rangle$, then the following relation between entanglement entropies holds:

$$\begin{aligned} E(v_1^\partial|v_2^\partial) &= \sum_j \tilde{\rho}_j \ln(2j+1) - \sum_j \tilde{\rho}_j \ln \tilde{\rho}_j \\ &\quad + \sum_j \tilde{\rho}_j E_j(v_1|v_2), \end{aligned} \quad (36)$$

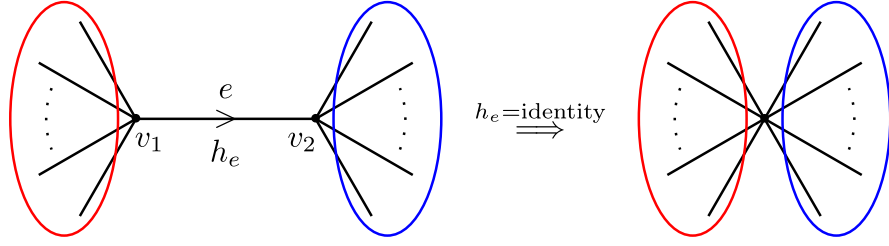


FIG. 2. The left graph (two vertices) has the same entanglement entropy between boundary edges with the right graph (one vertex).

where $E(v_1^d|v_2^d) := -\text{Tr}(\tilde{\rho}_{v_1}^d \ln \tilde{\rho}_{v_1}^d)$ and $E_j(v_1|v_2) = -\text{Tr}(\rho_{v_1}^j \ln \rho_{v_1}^j)$.

Let us have a discussion on the above theorem. First, referring to Ref. [57], the first term in Eq. (36) should be interpreted as coming from gauge breaking, and it follows that the second and the third terms should be interpreted as the intertwiner entanglement, since the $-\sum_j \tilde{p}_j \ln \tilde{p}_j$ comes from the spin superposition along the linking edge e , and the $E_j(v_1|v_2)$ is the intertwiner entanglement when the spin is fixed. Second, in the case of single internal edge graph, it has been shown that the holonomy along the internal edge e plays no role in the entanglement entropy in Ref. [57] for fixed j , and Eq. (33) in our calculation extends this point to the case of superposed j . Indeed, one is able to gauge fix the h_e into identity, and then $|\Psi_\Gamma\rangle_\delta$ becomes $|\check{\Psi}_\Gamma\rangle_\delta$, which can be regarded as an intertwiner on a single vertex as illustrated in Fig. 2. Notice that Eq. (33) tells us that $|\Psi_\Gamma\rangle_\delta$ and $|\check{\Psi}_\Gamma\rangle_\delta$ have the same reduced density matrix; thus, the respected entanglement entropies depicted in Fig. 2 are indistinguishable. Third, while the above general formalism is still vague for the sake of establishing a relation between the entanglement and geometry, the coherent intertwiners provide a semiclassical picture of geometry on the polyhedron, which could interlace the genuine quantum notion—entanglement, with the discrete geometry. In the following part of this paper, we are going to explore how the entanglement entropy emerges from this semiclassical picture and how the entanglement gets reflected in the discrete geometry, or vice versa.

B. Entanglement produced from group averaging

As a prelude for the study on the coherent intertwiner, this part is meant to show how entanglement can be produced from group averaging. We begin with a gauge-variant scenario based on the graph with only one vertex v , and the corresponding wave function is below the tensor state,

$$\bigotimes_{e|t(e)=v} |j_e, m_e\rangle \otimes \bigotimes_{e|s(e')=v} \langle j_{e'}, m_{e'}| \in \bigotimes_{e|t(e)=v} V^{j_e} \otimes \bigotimes_{e|s(e')=v} \bar{V}^{j_{e'}}. \quad (37)$$

This is not a physical spin network due to the absence of gauge invariance, and there is also no entanglement. To get a gauge-invariant state, the group averaging is adopted, which inevitably introduces superposition and entanglement. It is possible to grant the physical implication for the group averaging by considering some $SU(2)$ -invariant measurement: suppose that we are given a set $\{|\phi_i\rangle\}_i$ whose members are all $SU(2)$ -invariant pointer states $|\phi_i\rangle$; i.e., $|\phi_i\rangle = g|\phi_i\rangle$ for any $g \in SU(2)$, then this invariance can be conveyed to the probability distribution $|\langle \phi_i | \psi \rangle|^2$ where $|\psi\rangle$ is the state to be observed because

$$\begin{aligned} \langle \phi_i | \psi \rangle &= \int_{SU(2)} dg \langle g\phi_i | \psi \rangle = \int_{SU(2)} dg \langle \phi_i | g^\dagger \psi \rangle \\ &= \langle \phi_i | \int_{SU(2)} dg |g^\dagger \psi\rangle. \end{aligned} \quad (38)$$

It is clear that $\int_{SU(2)} dg |g^\dagger \psi\rangle$ is $SU(2)$ invariant. Note that this group-averaging process is similar to a particular “twirling” in the field of quantum information, which introduces superposition and entanglement to a product state.

The rest of this part will calculate the entanglement introduced by the group averaging. Let us look at an example. Consider the graph with only one 4-valents’ vertex v and the intertwiner space $\check{\mathcal{H}}_v^{\{j_1, j_2, j_3, j_4\}} = V^{j_1} \otimes V^{j_2} \otimes \bar{V}^{j_3} \otimes \bar{V}^{j_4}$ on v . An element in $\check{\mathcal{H}}_v^{\{j_1, j_2, j_3, j_4\}}$ is given by the tensor product as

$$|j_1, m_1\rangle \otimes |j_2, m_2\rangle \otimes \langle j_3, m_3| \otimes \langle j_4, m_4|, \quad (39)$$

where we take the 4-valents’ bipartition (2, 2), with the two left-side edges being ingoing and the two right-side edges being outgoing. Clearly, there is no entanglement between left and right sides, say, $E(A|B) = 0$ with $\mathcal{H}_A := V^{j_1} \otimes V^{j_2}$ and $\mathcal{H}_B := \bar{V}^{j_3} \otimes \bar{V}^{j_4}$. Now, let us implement the $SU(2)$ -group averaging over the tensor state, which leads to

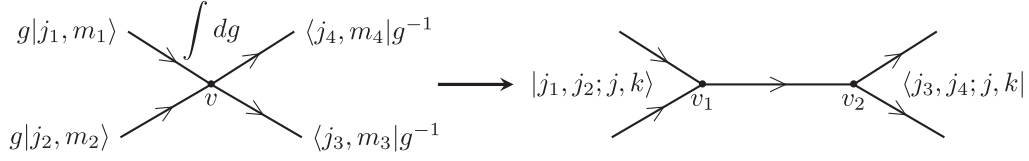


FIG. 3. The $SU(2)$ -group averaging produces entanglement between the legs. This can be viewed as the entanglement between two coupled states $|j_1, j_2; j, k\rangle$ and $\langle j_3, j_4; j, k|$ at v_1 and v_2 , respectively.

$$\begin{aligned}
 |\check{\mathcal{L}}\rangle &= \int_{SU(2)} dg g|j_1, m_1\rangle \otimes g|j_2, m_2\rangle \otimes \langle j_3, m_3|g^{-1} \\
 &\quad \otimes \langle j_4, m_4|g^{-1} \\
 &= \sum_j \sum_{k, m=-j}^j \sum_{\vec{k}} \frac{1}{2j+1} C_{k_1 k_2 k}^{j_1 j_2 j} \overline{C_{m_1 m_2 m}^{j_1 j_2 j}} \overline{C_{k_3 k_4 k}^{j_3 j_4 j}} \\
 &\quad \times C_{m_3 m_4 m}^{j_3 j_4 j} |j_1, k_1\rangle \otimes |j_2, k_2\rangle \otimes \langle j_3, k_3| \otimes \langle j_4, k_4|,
 \end{aligned} \tag{40}$$

where $\vec{k} \equiv \{k_1, k_2, k_3, k_4\}$ and $C_{m_1 m_2 m}^{j_1 j_2 j} \equiv \langle j_1, m_1, j_2, m_2 | j, m\rangle$ stands for the Clebsch-Gordan coefficient. One should note that the group averaging spoils the normalization, so it

should be retrieved by rescaling later. In addition, recall that $\vec{m} \equiv \{m_1, m_2, m_3, m_4\}$ are fixed, the $SU(2)$ -group averaging will eliminate some configurations that do not satisfy $m_1 + m_2 = m_3 + m_4$. This is the closure condition on magnetic quantum numbers. The state $|\check{\mathcal{L}}\rangle$ survived from the group averaging is a gauge-invariant state, and it can be also viewed as a bipartite system between two sets of recoupled spins; see the illustration in Fig. 3. To simplify the expression, let us rewrite $|\check{\mathcal{L}}\rangle$ as

$$|\check{\mathcal{L}}\rangle = \sum_{j, k} \frac{1}{2j+1} f(j, \vec{j}, \vec{m}) |j_1, j_2; j, k\rangle \otimes \langle j_3, j_4; j, k|, \tag{41}$$

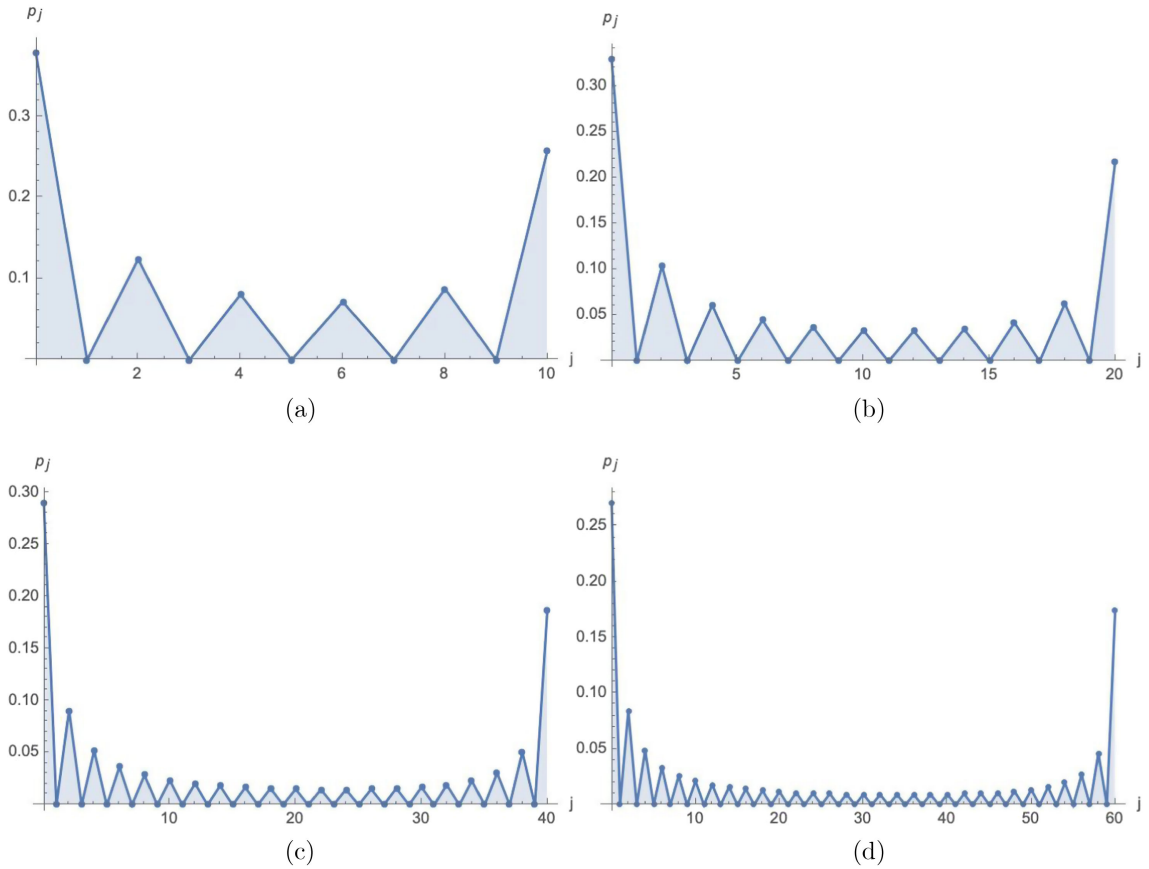


FIG. 4. The numerical results of p_j for $(m_1, m_2, m_3, m_4) = (0, 0, 0, 0)$ and $j_1 = j_2 = j_3 = j_4 = 5, 10, 20, 30$, where the x axis shows the recoupling spin j and the y axis shows the numerical value of p_j . These figures show that p_j has an oscillation with respect to coupling spin j . (a) $j_1 = j_2 = j_3 = j_4 = 5$. (b) $j_1 = j_2 = j_3 = j_4 = 10$. (c) $j_1 = j_2 = j_3 = j_4 = 20$. (d) $j_1 = j_2 = j_3 = j_4 = 30$.

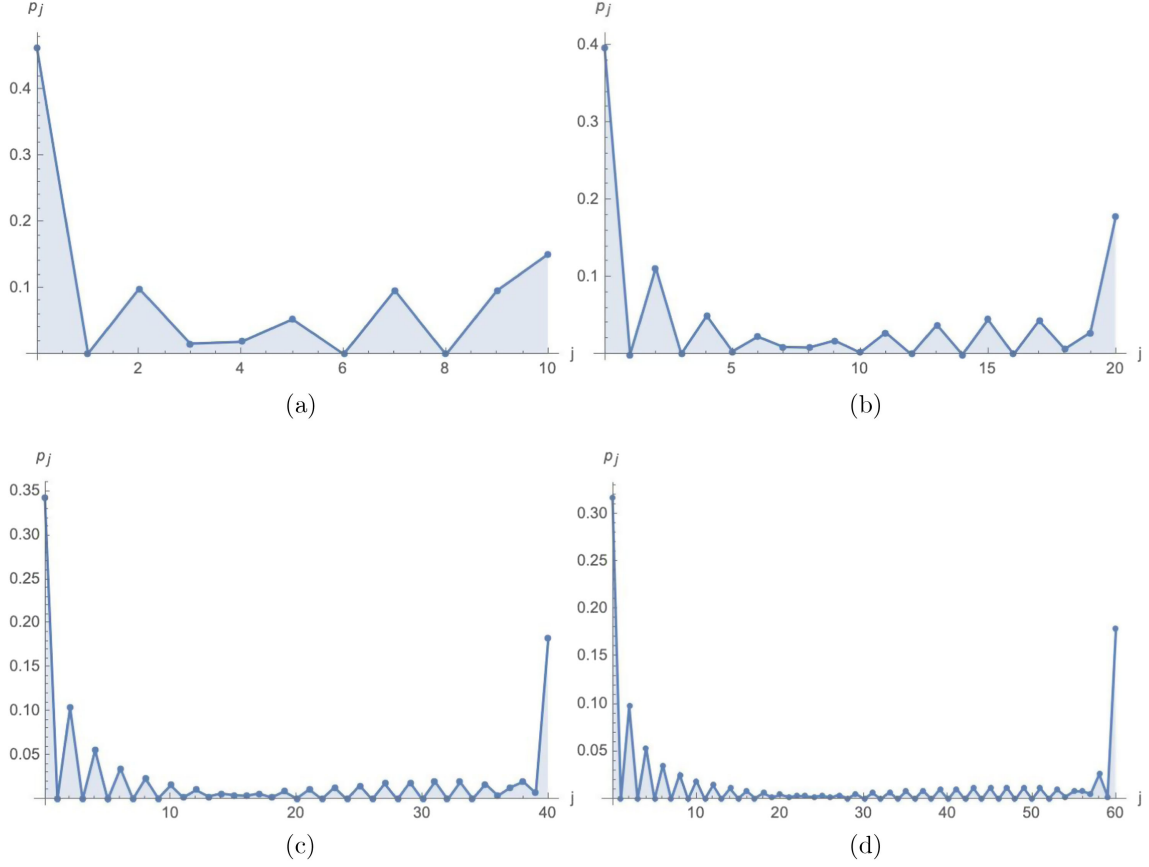


FIG. 5. The numerical results of p_j for $(m_1, m_2, m_3, m_4) = (1, -1, 1, -1)$ and $j_1 = j_2 = j_3 = j_4 = 5, 10, 20, 30$, where the x axis shows the recouping spin j and y axis shows the numerical value of p_j . These figures show the difference in the shape of oscillation compared to the cases of $m_1 = m_2 = m_3 = m_4 = 0$. (a) $j_1 = j_2 = j_3 = j_4 = 5$. (b) $j_1 = j_2 = j_3 = j_4 = 10$. (c) $j_1 = j_2 = j_3 = j_4 = 20$. (d) $j_1 = j_2 = j_3 = j_4 = 30$.

where $|j_1, j_2; j, k\rangle := \sum_{\{k_1, k_2\}} C_{k_1 k_2 k}^{j_1 j_2 j} |j_1, k_1\rangle \otimes |j_2, k_2\rangle$ defines a recoupled spin, likewise for $\langle j_3, j_4; j, k|$, and we denote

$$f(j, \vec{j}, \vec{m}) \equiv \sum_m \overline{C_{m_1 m_2 m}^{j_1 j_2 j}} C_{m_3 m_4 m}^{j_3 j_4 j} \quad (42)$$

for the fixed $\vec{j} \equiv \{j_1, j_2, j_3, j_4\}$ and \vec{m} .

Recall the bipartition $\mathcal{H}_A := V^{j_1} \otimes V^{j_2}$ and $\mathcal{H}_B := V^{j_3} \otimes V^{j_4}$. Then, the entanglement $E(A|B)$ between A and B can be given by the von Neumann entropy of the reduced density matrices ρ_A . For the state $|\check{\mathcal{I}}\rangle$, the reduced density matrix ρ_A is defined by $\rho_A := \text{Tr}_B(\rho_{\check{\mathcal{I}}})$ with $\rho_{\check{\mathcal{I}}} \equiv \frac{|\check{\mathcal{I}}\rangle\langle\check{\mathcal{I}}|}{\langle\check{\mathcal{I}}|\check{\mathcal{I}}\rangle}$. More explicitly, one has

$$\rho_A = \frac{1}{\langle\check{\mathcal{I}}|\check{\mathcal{I}}\rangle} \sum_j \sum_{k=-j}^j \frac{|f(j, \vec{j}, \vec{m})|^2}{(2j+1)^2} |j_1, j_2; j, k\rangle\langle j_1, j_2; j, k|. \quad (43)$$

One can introduce the probability distribution p_j of the recouping spin j , which is given by $p_j = \frac{|f(j, \vec{j}, \vec{m})|^2}{(2j+1)\langle\check{\mathcal{I}}|\check{\mathcal{I}}\rangle}$,

and the reduced density matrix can be decomposed into ρ_j^A , i.e.,

$$\rho_A = \sum_j p_j \rho_j^A, \quad \rho_j^A = \sum_{k=-j}^j \frac{|j_1, j_2; j, k\rangle\langle j_1, j_2; j, k|}{(2j+1)}. \quad (44)$$

It is clear that the \mathcal{H}_A and \mathcal{H}_B are entangled for the state $|\check{\mathcal{I}}\rangle$. The entanglement entropy $E(A|B) := -\text{Tr}(\rho_A \ln \rho_A)$ is determined by the distribution p_j , which reads

$$E(A|B) = E_p(A|B) + E_0(A|B), \quad E_p(A|B) := -\sum_j (p_j \ln p_j), \quad E_0(A|B) := \sum_j p_j S_j^A, \quad (45)$$

where $S_j^A := -\text{Tr}(\rho_j^A \ln \rho_j^A) = \ln(2j+1)$. Further, the distribution p_j and the entanglement entropy $E(A|B)$ can be calculated numerically. The numerical results of p_j are illustrated in Figs. 4–6, which show that the distribution p_j is oscillating with respect to j for small $\{m_1, m_2, m_3, m_4\}$ state, while there is a peak for highest (and lowest) weight state. The numerical values of entanglement entropy

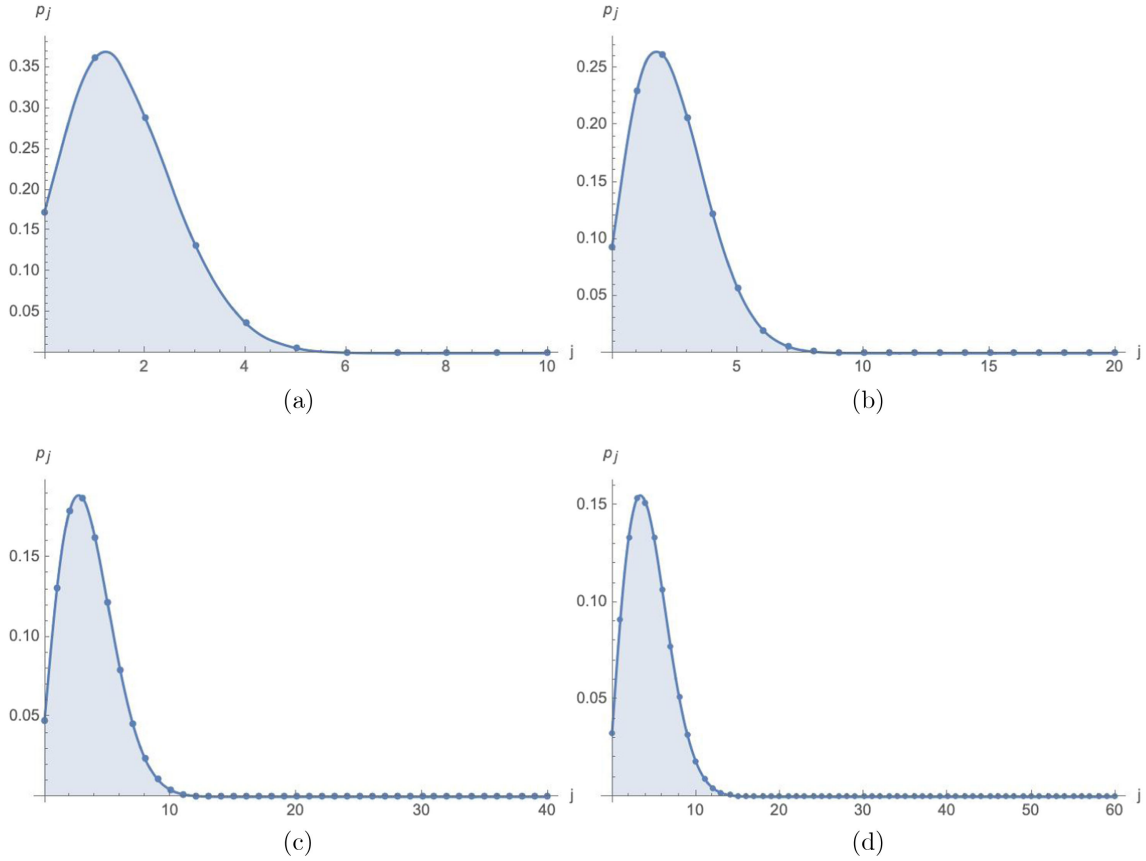


FIG. 6. The numerical results of p_j for $j_1 = j_2 = j_3 = j_4 = 5, 10, 20, 30$ and $m_1 = m_3 = -m_2 = -m_4 = j_4$, where the x axis shows the recoupling spin j and the y axis shows the numerical value of p_j . These figures show that the shapes of the distributions p_j are peaks for the highest (and lowest) weight states. (a) $j_1 = j_2 = j_3 = j_4 = 5$. (b) $j_1 = j_2 = j_3 = j_4 = 10$. (c) $j_1 = j_2 = j_3 = j_4 = 20$. (d) $j_1 = j_2 = j_3 = j_4 = 30$.

$E(A|B)$ are listed in Tables I and II, which show that the entanglement entropy can be controlled by the magnetic configurations.

It is worth it to have a discussion on these results. First, one should notice that the quantum number $\{m_1, m_2, m_3, m_4\}$ are gauge variant, and their geometric

interpretation become fuzzy after group averaging. Second, note that the distribution p_j is a peak for highest (and lowest) weight state; it ensures that the entanglement entropy is able to capture the main character of the distribution p_j . By combining these two points, it is

TABLE I. The numerical values of $E(A|B)$ for small spins $j_1 = j_2 = j_3 = j_4 = 5$ at different configurations with respect to magnetic numbers.

(j_1, j_2, j_3, j_4)	(m_1, m_2, m_3, m_4)	$E_p(A B)$	$E_0(A B)$	$E(A B)$
(5, 5, 5, 5)	(0, 0, 0, 0)	1.58138	1.5931	3.17448
(5, 5, 5, 5)	(1, -1, 1, -1)	1.64349	1.37831	3.0218
(5, 5, 5, 5)	(2, -2, 2, -2)	1.68047	1.35532	3.03579
(5, 5, 5, 5)	(3, -3, 3, -3)	1.72176	1.33854	3.06029
(5, 5, 5, 5)	(4, -4, 4, -4)	1.6484	1.30671	2.95511
(5, 5, 5, 5)	(5, -5, 5, -5)	1.45701	1.21724	2.67426
(5, 5, 5, 5)	(2, -1, 2, -1)	1.7005	2.05912	3.75962
(5, 5, 5, 5)	(3, -1, 3, -1)	1.77649	2.32768	4.10417
(5, 5, 5, 5)	(4, -1, 4, -1)	1.59752	2.48947	4.08698
(5, 5, 5, 5)	(5, -1, 5, -1)	1.31356	2.60331	3.91687

TABLE II. The numerical values of $E(A|B)$ for small spins $j_1 = j_2 = j_3 = j_4 = 10$ at different configurations with respect to magnetic numbers.

(j_1, j_2, j_3, j_4)	(m_1, m_2, m_3, m_4)	$E_p(A B)$	$E_0(A B)$	$E(A B)$
(10, 10, 10, 10)	(0, 0, 0, 0)	2.01747	2.02953	4.047
(10, 10, 10, 10)	(1, -1, 1, -1)	2.01367	1.80432	3.81799
(10, 10, 10, 10)	(2, -2, 2, -2)	2.06684	1.77726	3.8441
(10, 10, 10, 10)	(3, -3, 3, -3)	2.10459	1.76694	3.87153
(10, 10, 10, 10)	(4, -4, 4, -4)	2.1037	1.76034	3.86404
(10, 10, 10, 10)	(5, -5, 5, -5)	2.13296	1.75342	3.88638
(10, 10, 10, 10)	(6, -6, 6, -6)	2.16708	1.7438	3.91088
(10, 10, 10, 10)	(7, -7, 7, -7)	2.1329	1.72895	3.86185
(10, 10, 10, 10)	(8, -8, 8, -8)	2.08743	1.70467	3.7921
(10, 10, 10, 10)	(9, -9, 9, -9)	1.99391	1.66086	3.65477
(10, 10, 10, 10)	(10, -10, 10, -10)	1.77857	1.55688	3.33545

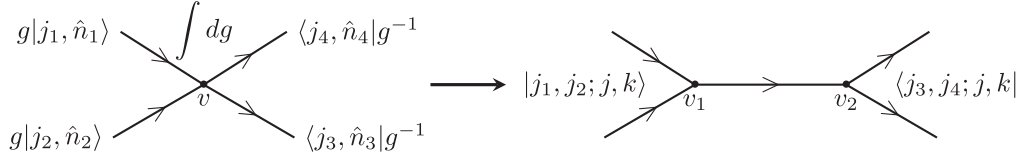


FIG. 7. The $SU(2)$ -group averaging on spin coherent state produces entanglement between the legs. This can be viewed as the entanglement between two coupled states $|j_1, j_2; j, k\rangle$ and $\langle j_3, j_4; j, k|$ at v_1 and v_2 , respectively.

reasonable to consider the entanglement carried by gauge-invariant coherent intertwiners, since they are constructed by the highest (and lowest) weight state and they describe semiclassical geometry on polyhedrons. In the next subsection, we will focus on the coherent intertwiners which provide a semiclassical picture of polyhedron geometry, and one may expect that the entanglement, superposition, and the geometric picture could be drawn by the gauge-invariant knowledge encoded in the area-weighted normal vectors $\{j_e \hat{n}_e\}$ labeling the coherent intertwiners.

C. Entanglement entropy between legs of coherent intertwiner

1. Coherent intertwiner with four legs

Let us consider the gauge-invariant coherent intertwiner space $\mathcal{H}_v^{\{j_1, j_2, j_3, j_4\}} = \text{Inv}_{SU(2)}[V^{j_1} \otimes V^{j_2} \otimes \bar{V}^{j_3} \otimes \bar{V}^{j_4}]$ on a 4-valents vertex, in which an element is given by

$$|\mathcal{I}\rangle = \int_{SU(2)} dg g|j_1, \hat{n}_1\rangle \otimes g|j_2, \hat{n}_2\rangle \otimes \langle j_3, \hat{n}_3|g^{-1} \otimes \langle j_4, \hat{n}_4|g^{-1}, \quad (46)$$

wherein the spins and vectors satisfy the closure condition $j_1 \hat{n}_1 + j_2 \hat{n}_2 = j_3 \hat{n}_3 + j_4 \hat{n}_4$. Now, let us start to calculate the entanglement entropy for $|\mathcal{I}\rangle$. By recalling Eq. (11), the state is then rewritten in the manner of repeating Eq. (40) as illustrated in Fig. 7, which reads

$$\begin{aligned} |\mathcal{I}\rangle &= \sum_{\vec{m}} c_{j_1, m_1}(\hat{n}_1) c_{j_2, m_2}(\hat{n}_2) \bar{c}_{j_3, m_3}(\hat{n}_3) \bar{c}_{j_4, m_4}(\hat{n}_4) \\ &\cdot \int_{SU(2)} dg g|j_1, m_1\rangle \otimes g|j_2, m_2\rangle \otimes \langle j_3, m_3|g^{-1} \\ &\otimes \langle j_4, m_4|g^{-1} \\ &= \sum_{\vec{m}} c_{j_1, m_1}(\hat{n}_1) c_{j_2, m_2}(\hat{n}_2) \bar{c}_{j_3, m_3}(\hat{n}_3) \bar{c}_{j_4, m_4}(\hat{n}_4) \\ &\times \sum_{j, m, k} \frac{\overline{C_{m_1 m_2 m}^{j_1 j_2 j}} C_{m_3 m_4 m}^{j_3 j_4 j}}{2j+1} |j_1, j_2; j, k\rangle \otimes \langle j_3, j_4; j, k|, \end{aligned} \quad (47)$$

$$= \sum_{j, m, k} \frac{C_{\hat{n}_1 \hat{n}_2 m}^{j_1 j_2 j} \overline{C_{\hat{n}_3 \hat{n}_4 m}^{j_3 j_4 j}}}{2j+1} |j_1, j_2; j, k\rangle \otimes \langle j_3, j_4; j, k|, \quad (48)$$

where the ranges of the sums are given by $-j \leq m, k \leq j$, $\max(|j_1 - j_2|, |j_3 - j_4|) \leq j \leq \min((j_1 + j_2), (j_3 + j_4))$; the second line uses the recoupled spins $|j_1, j_2; j, k\rangle := \sum_{m_1, m_2} C_{m_1 m_2 k}^{j_1 j_2 j} |j_1, m_1\rangle \otimes |j_2, m_2\rangle$ and $\langle j_3, j_4; j, k| := \sum_{m_3, m_4} \overline{C_{m_3 m_4 k}^{j_3 j_4 j}} \langle j_3, m_3| \otimes \langle j_4, m_4|$; and in the third line we have denoted

$$C_{\hat{n}_1 \hat{n}_2 m}^{j_1 j_2 j} \equiv \sum_{m_1=-j_1}^{j_1} \sum_{m_2=-j_2}^{j_2} c_{j_1, m_1}(\hat{n}_1) c_{j_2, m_2}(\hat{n}_2) \overline{C_{m_1 m_2 m}^{j_1 j_2 j}}, \quad (49)$$

$$\overline{C_{\hat{n}_3 \hat{n}_4 m}^{j_3 j_4 j}} \equiv \sum_{m_3=-j_3}^{j_3} \sum_{m_4=-j_4}^{j_4} \bar{c}_{j_3, m_3}(\hat{n}_3) \bar{c}_{j_4, m_4}(\hat{n}_4) C_{m_3 m_4 m}^{j_3 j_4 j}. \quad (50)$$

TABLE III. The numerical values of $E_p(A|B)$ and $E_0(A|B)$ for fixed $\hat{n}_1, \hat{n}_2, \hat{n}_3, \hat{n}_4$ and growth boundary spins, where $\hat{n}_1 = (\sin \theta_1 \cos \varphi_1, \sin \theta_1 \sin \varphi_1, \cos \theta_1)$ and likewise for $\hat{n}_2, \hat{n}_3, \hat{n}_4$. It is shown that $E_p(A|B)$ and $E_0(A|B)$ both grow with the boundary spins $j_1 = j_2 = j_3 = j_4$ getting larger.

(j_1, j_2, j_3, j_4)	$(\theta_1, \theta_2, \theta_3, \theta_4)$	$(\varphi_1, \varphi_2, \varphi_3, \varphi_4)$	$E_p(A B)$	$E_0(A B)$	$E(A B)$
(5, 5, 5, 5)	$(\frac{\pi}{2}, \frac{\pi}{2}, \frac{\pi}{4}, \frac{3\pi}{4})$	$(0, \frac{\pi}{2}, \frac{\pi}{4}, \frac{\pi}{4})$	1.56229	2.70936	4.27165
(10, 10, 10, 10)	$(\frac{\pi}{2}, \frac{\pi}{2}, \frac{\pi}{4}, \frac{3\pi}{4})$	$(0, \frac{\pi}{2}, \frac{\pi}{4}, \frac{\pi}{4})$	1.8922	3.37298	5.26517
(15, 15, 15, 15)	$(\frac{\pi}{2}, \frac{\pi}{2}, \frac{\pi}{4}, \frac{3\pi}{4})$	$(0, \frac{\pi}{2}, \frac{\pi}{4}, \frac{\pi}{4})$	2.08976	3.76835	5.85811
(20, 20, 20, 20)	$(\frac{\pi}{2}, \frac{\pi}{2}, \frac{\pi}{4}, \frac{3\pi}{4})$	$(0, \frac{\pi}{2}, \frac{\pi}{4}, \frac{\pi}{4})$	2.23109	4.05092	6.28201
(25, 25, 25, 25)	$(\frac{\pi}{2}, \frac{\pi}{2}, \frac{\pi}{4}, \frac{3\pi}{4})$	$(0, \frac{\pi}{2}, \frac{\pi}{4}, \frac{\pi}{4})$	2.34114	4.271	6.61214
(30, 30, 30, 30)	$(\frac{\pi}{2}, \frac{\pi}{2}, \frac{\pi}{4}, \frac{3\pi}{4})$	$(0, \frac{\pi}{2}, \frac{\pi}{4}, \frac{\pi}{4})$	2.43131	4.45127	6.88258

TABLE IV. The numerical values of $E_p(A|B)$ and $E_0(A|B)$ for fixed boundary spins $j_1 = j_2 = j_3 = j_4 = 20$ and various angle $\arccos(\hat{n}_1 \cdot \hat{n}_2) = \varphi_2 - \varphi_1$. It is shown that $E_p(A|B)$ increases while $E_0(A|B)$ decreases with the angle $\arccos(\hat{n}_1 \cdot \hat{n}_2)$ getting larger.

(j_1, j_2, j_3, j_4)	$(\theta_1, \theta_2, \theta_3, \theta_4)$	$(\varphi_1, \varphi_2, \varphi_3, \varphi_4)$	$E_p(A B)$	$E_0(A B)$	$E(A B)$
(20, 20, 20, 20)	$(\frac{\pi}{2}, \frac{\pi}{2}, \frac{7\pi}{16}, \frac{9\pi}{16})$	$(0, \frac{\pi}{8}, \frac{\pi}{16}, \frac{\pi}{16})$	0.861644	4.38243	5.24407
(20, 20, 20, 20)	$(\frac{\pi}{2}, \frac{\pi}{2}, \frac{3\pi}{8}, \frac{5\pi}{8})$	$(0, \frac{\pi}{4}, \frac{\pi}{8}, \frac{\pi}{8})$	1.6089	4.3212	5.9301
(20, 20, 20, 20)	$(\frac{\pi}{2}, \frac{\pi}{2}, \frac{\pi}{4}, \frac{3\pi}{4})$	$(0, \frac{\pi}{2}, \frac{\pi}{4}, \frac{\pi}{4})$	2.23109	4.05092	6.28201
(20, 20, 20, 20)	$(\frac{\pi}{2}, \frac{\pi}{2}, \frac{\pi}{6}, \frac{5\pi}{6})$	$(0, \frac{2\pi}{3}, \frac{\pi}{3}, \frac{\pi}{3})$	2.43579	3.69809	6.13388
(20, 20, 20, 20)	$(\frac{\pi}{2}, \frac{\pi}{2}, \frac{\pi}{8}, \frac{7\pi}{8})$	$(0, \frac{3\pi}{4}, \frac{3\pi}{8}, \frac{3\pi}{8})$	2.50054	3.42048	5.92102
(20, 20, 20, 20)	$(\frac{\pi}{2}, \frac{\pi}{2}, \frac{\pi}{16}, \frac{15\pi}{16})$	$(0, \frac{7\pi}{8}, \frac{7\pi}{16}, \frac{7\pi}{16})$	2.541	2.65329	5.1943

The density matrix of the coherent intertwiner $|\mathcal{I}\rangle$ is given by $\rho_{\mathcal{I}} \equiv \frac{|\mathcal{I}\rangle\langle\mathcal{I}|}{\langle\mathcal{I}|\mathcal{I}\rangle}$ where its denominator, namely, the normalization factor, is given by

$$\langle\mathcal{I}|\mathcal{I}\rangle = \sum_j \frac{1}{2j+1} \left| \sum_m C_{\hat{n}_1 \hat{n}_2 m}^{j_1 j_2 j} \overline{C_{\hat{n}_3 \hat{n}_4 m}^{j_3 j_4 j}} \right|^2. \quad (51)$$

Recall the definitions $\mathcal{H}_A := V^{j_1} \otimes V^{j_2}$ and $\mathcal{H}_B := \bar{V}^{j_3} \otimes \bar{V}^{j_4}$. Then, for the state $|\mathcal{I}\rangle$, the entanglement $E(A|B)$ between A and B can be given by the von Neumann entropy of the reduced density matrices ρ_A , which are defined by

$$\rho_A := \text{Tr}_B(\rho_{\mathcal{I}}), \quad E(A|B) := -\text{Tr}(\rho_A \ln \rho_A). \quad (52)$$

More explicitly, ρ_A can be calculated as

$$\begin{aligned} \rho_A &= \text{Tr}_B(\rho_{\mathcal{I}}) \\ &= \sum_j \frac{1}{2j+1} \frac{\left| \sum_m C_{\hat{n}_1 \hat{n}_2 m}^{j_1 j_2 j} \overline{C_{\hat{n}_3 \hat{n}_4 m}^{j_3 j_4 j}} \right|^2}{\sum_{j'} \frac{1}{2j'+1} \left| \sum_{m'} C_{\hat{n}_1 \hat{n}_2 m'}^{j_1 j_2 j'} \overline{C_{\hat{n}_3 \hat{n}_4 m'}^{j_3 j_4 j'}} \right|^2} \\ &\quad \times \sum_{k=-j}^j \frac{|j_1, j_2; j, k\rangle\langle j_1, j_2; j, k|}{2j+1}, \end{aligned} \quad (53)$$

which can be also read in the form of

$$\begin{aligned} \rho_A &= \sum_j p_j \rho_j^A, \\ p_j &= \frac{\left| \sum_m C_{\hat{n}_1 \hat{n}_2 m}^{j_1 j_2 j} \overline{C_{\hat{n}_3 \hat{n}_4 m}^{j_3 j_4 j}} \right|^2}{(2j+1) \sum_{j'} \frac{1}{2j'+1} \left| \sum_{m'} C_{\hat{n}_1 \hat{n}_2 m'}^{j_1 j_2 j'} \overline{C_{\hat{n}_3 \hat{n}_4 m'}^{j_3 j_4 j'}} \right|^2}, \end{aligned} \quad (54)$$

and $\rho_j^A = \frac{\sum_k |j_1, j_2; j, k\rangle\langle j_1, j_2; j, k|}{(2j+1)}$. Further, we have

$$\begin{aligned} E(A|B) &= E_p(A|B) + E_0(A|B), \\ E_p(A|B) &:= -\sum_j (p_j \ln p_j), \quad E_0(A|B) := \sum_j p_j S_j^A, \end{aligned} \quad (55)$$

where $S_j^A \equiv -\text{Tr}(\rho_j^A \ln \rho_j^A) = \ln(2j+1)$ and $E_p(A|B) = -\sum_j (p_j \ln p_j)$ is just the Shannon entropy of the distribution p_j .

One can see that $E(A|B)$ is determined by the distribution p_j . Generally, p_j is a rather complicated function of j for given $(j_1, \hat{n}_1, j_2, \hat{n}_2, j_3, \hat{n}_3, j_4, \hat{n}_4)$; thus, it is hard to analyze the property of p_j by its analytical expression. We calculate p_j and $E(A|B)$ by the numerical methods as

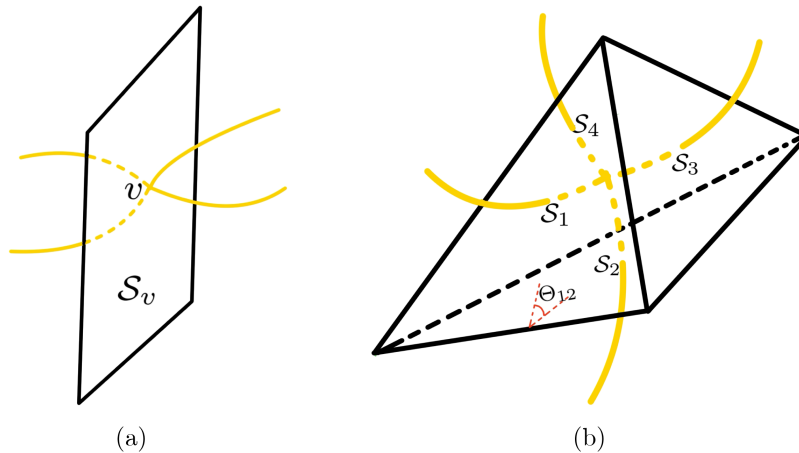


FIG. 8. Geometric interpretation of j_0, j_1, j_2, j_3, j_4 , and $\arccos(\hat{n}_1 \cdot \hat{n}_2)$ which are related to the entanglement of coherent intertwiner. (a) The face S_v punctured only by the 4-valents vertex v . (b) The face S_1, S_2, S_3, S_4 and the dihedral angle Θ_{12} between S_1 and S_2 .

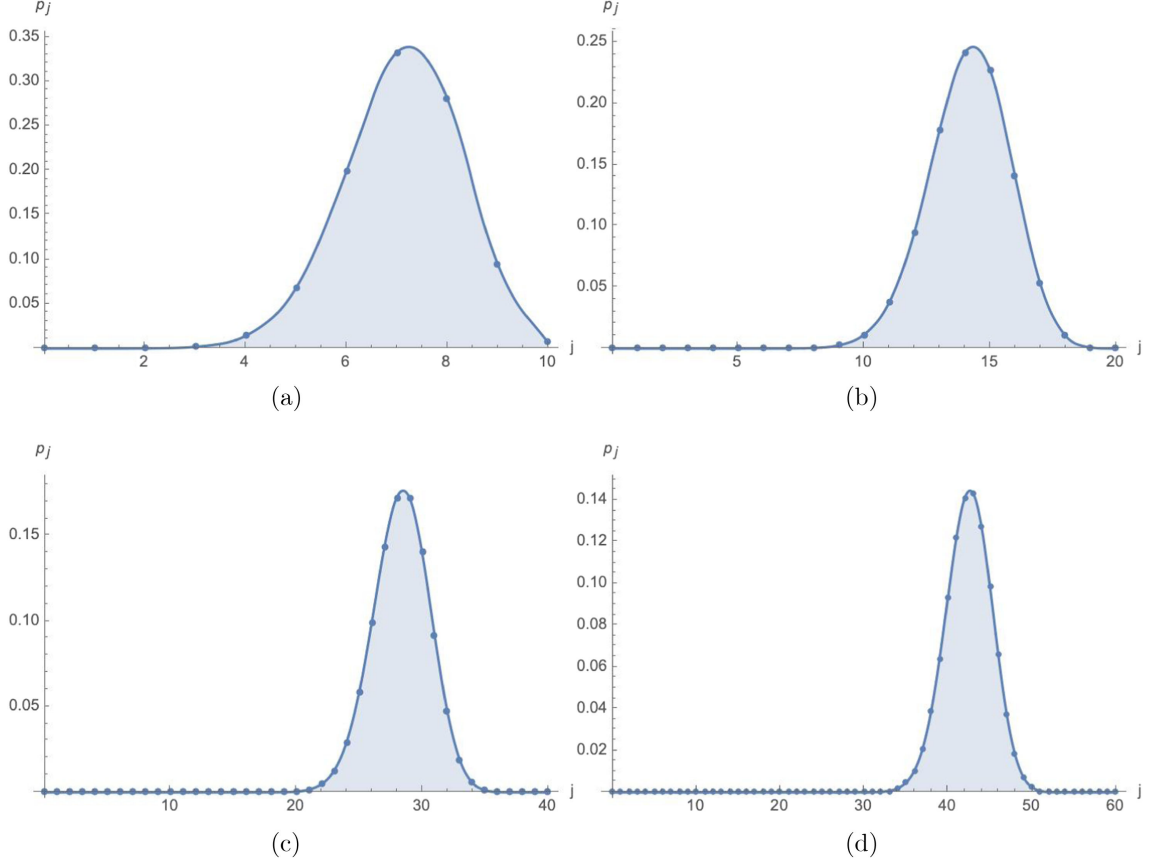


FIG. 9. The numerical results of p_j for $(\theta_1, \theta_2, \theta_3, \theta_4) = (\frac{\pi}{2}, \frac{\pi}{2}, \frac{\pi}{4}, \frac{3\pi}{4})$, $(\varphi_1, \varphi_2, \varphi_3, \varphi_4) = (0, \frac{\pi}{2}, \frac{\pi}{4}, \frac{\pi}{4})$, and $j_1 = j_2 = j_3 = j_4 = 5, 10, 20, 30$, where the x axis shows the recoupling spin j and the y axis shows the numerical value of p_j . These figures show that p_j has a peak near $j = j_0 \equiv |j_1 \hat{n}_1 + j_2 \hat{n}_2|$, and this peak shrinks relative to the range of j with the boundary spins j_1, j_2, j_3, j_4 getting larger. (a) $j_1 = j_2 = j_3 = j_4 = 5$. (b) $j_1 = j_2 = j_3 = j_4 = 10$. (c) $j_1 = j_2 = j_3 = j_4 = 20$. (d) $j_1 = j_2 = j_3 = j_4 = 30$.

shown in Tables III, IV, Figs. 9, and 10. Our results show that p_j has a peak near $j = j_0 \equiv |j_1 \hat{n}_1 + j_2 \hat{n}_2| = \sqrt{j_1^2 + j_2^2 + 2j_1 j_2 \hat{n}_1 \cdot \hat{n}_2}$ and thus one has $\sum_j j p_j \approx j_0$ and $E_0(A|B) = \sum_j p_j S_j^A \approx \ln(2j_0 + 1)$. Specifically, this peak shrinks relative to the range of j with the boundary spins j_1, j_2, j_3, j_4 getting larger as shown in Fig. 9, so $E_0(A|B)$ and $E_p(A|B)$ increases no more than logarithmic growth with j_1, j_2, j_3, j_4 going large as shown in Table III. Also, this peak shrinks with the angle $\arccos(\hat{n}_1 \cdot \hat{n}_2)$ decreasing, Fig. 10, and thus $E_p(A|B)$ increases with the angle $\arccos(\hat{n}_1 \cdot \hat{n}_2)$ getting larger, Table IV. Especially, for fixed $j_0 = \sqrt{j_1^2 + j_2^2 + 2j_1 j_2 \hat{n}_1 \cdot \hat{n}_2}$, one can increase j_1, j_2 , and the angle $\arccos(\hat{n}_1 \cdot \hat{n}_2)$ at the same time to grow $E_p(A|B)$ as shown in Tables III and IV.

It is worth it to explain the geometric interpretation of j_0, j_1, j_2, j_3, j_4 , and $\arccos(\hat{n}_1 \cdot \hat{n}_2)$ which is related to the entanglement. As shown in Fig. 8, let us consider the face \mathcal{S}_v punctured only by the 4-valents vertex v labeled by $|\mathcal{I}\rangle$, with two legs of v lying in one side and the other two legs in another side of \mathcal{S}_v . Then, the expectation value of the area of \mathcal{S}_v is given by

$$\begin{aligned} \text{Ar}(\mathcal{S}_v) &\equiv \langle \check{\mathcal{I}} | \widehat{\text{Ar}}(\mathcal{S}_v) | \check{\mathcal{I}} \rangle \\ &:= 8\pi\beta\ell_{\text{pl}}^2 \langle \check{\mathcal{I}} | \sqrt{(\vec{J}_1 + \vec{J}_2) \cdot (\vec{J}_1 + \vec{J}_2)} | \check{\mathcal{I}} \rangle \approx 8\pi\beta\ell_{\text{pl}}^2 j_0, \end{aligned} \quad (56)$$

where $|\check{\mathcal{I}}\rangle := \frac{|\mathcal{I}\rangle}{\sqrt{\langle \mathcal{I} | \mathcal{I} \rangle}}$ is the normalized version of $|\mathcal{I}\rangle$, β is the Barbero-Immirzi parameter in LQG, and ℓ_{pl} is the Plank length. Besides, as shown in Fig. 8, one can also consider the area of the face \mathcal{S}_1 punctured only by the leg of the vertex v labeled by j_1 , which is given by the eigenvalue $\text{Ar}(\mathcal{S}_1) = 8\pi\beta\ell_{\text{pl}}^2 \sqrt{j_1(j_1 + 1)}$ following the eigenequation

$$\widehat{\text{Ar}}(\mathcal{S}_1) | \check{\mathcal{I}} \rangle := 8\pi\beta\ell_{\text{pl}}^2 \sqrt{\vec{J}_1 \cdot \vec{J}_1} | \check{\mathcal{I}} \rangle \approx 8\pi\beta\ell_{\text{pl}}^2 \sqrt{j_1(j_1 + 1)} | \check{\mathcal{I}} \rangle. \quad (57)$$

Similar results can be given for the faces $\mathcal{S}_2, \mathcal{S}_3, \mathcal{S}_4$ punctured only by the legs of the vertex v labeled by j_1, j_2, j_3 , respectively. Moreover, one can also define the angle

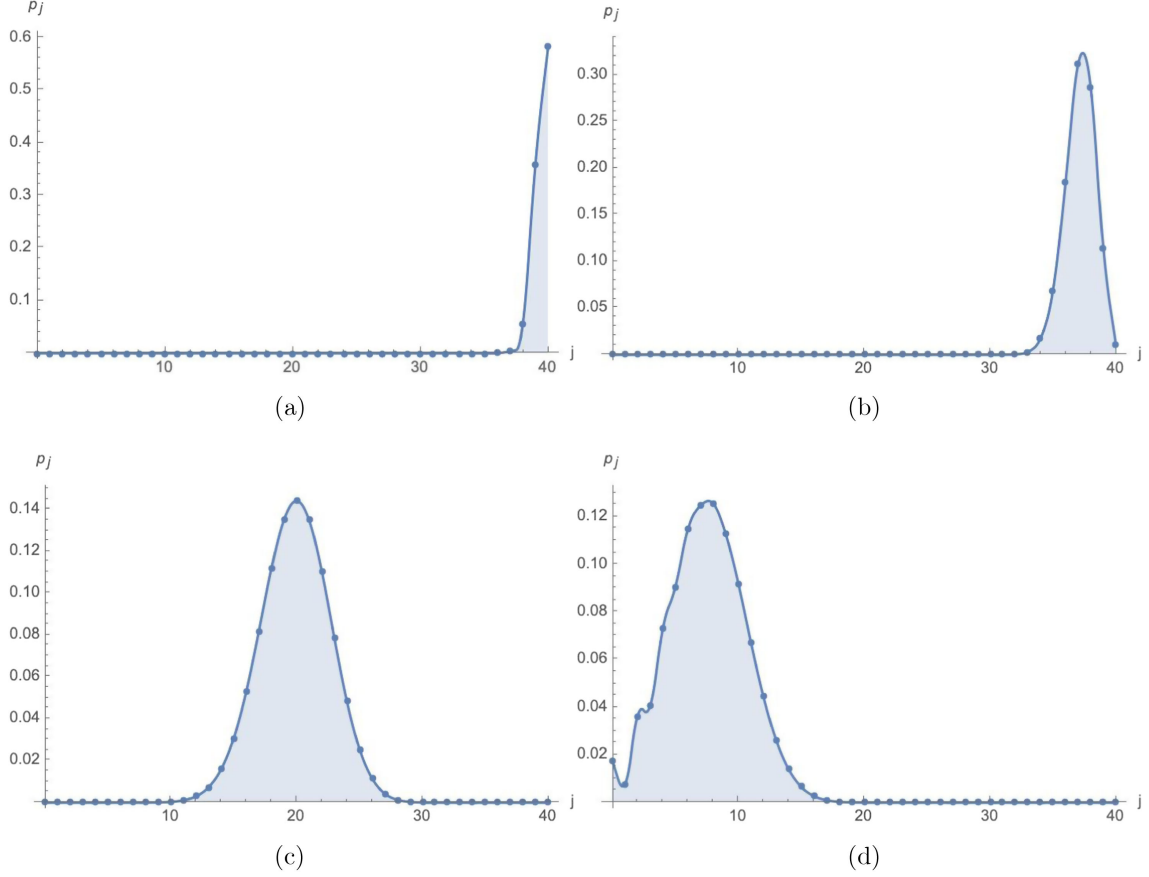


FIG. 10. The numerical results of p_j for $j_1 = j_2 = j_3 = j_4 = 20$ and various $\vec{\theta} \equiv (\theta_1, \theta_2, \theta_3, \theta_4)$, $\vec{\varphi} \equiv (\varphi_1, \varphi_2, \varphi_3, \varphi_4)$, where the x axis shows the recoupling spin j and the y axis shows the numerical value of p_j . These figures show that p_j has a peak near $j = j_0 \equiv |j_1 \hat{n}_1 + j_2 \hat{n}_2|$, and this peak shrinks with the angle $\arccos(\hat{n}_1 \cdot \hat{n}_2)$ decreasing. (a) $\vec{\theta} = (\frac{\pi}{2}, \frac{\pi}{2}, \frac{7\pi}{16}, \frac{9\pi}{16})$, $\vec{\varphi} = (0, \frac{\pi}{8}, \frac{\pi}{16}, \frac{\pi}{16})$. (b) $\vec{\theta} = (\frac{\pi}{2}, \frac{\pi}{2}, \frac{3\pi}{8}, \frac{5\pi}{8})$, $\vec{\varphi} = (0, \frac{\pi}{4}, \frac{\pi}{8}, \frac{\pi}{8})$. (c) $\vec{\theta} = (\frac{\pi}{2}, \frac{\pi}{2}, \frac{\pi}{6}, \frac{5\pi}{6})$, $\vec{\varphi} = (0, \frac{2\pi}{3}, \frac{\pi}{3}, \frac{\pi}{3})$. (d) $\vec{\theta} = (\frac{\pi}{2}, \frac{\pi}{2}, \frac{\pi}{16}, \frac{15\pi}{16})$, $\vec{\varphi} = (0, \frac{7\pi}{8}, \frac{7\pi}{16}, \frac{7\pi}{16})$.

between the faces \mathcal{S}_1 and \mathcal{S}_2 ; then, the expectation value of this angle is given by

$$\begin{aligned} \Theta_{12} &\equiv \langle \check{\mathcal{I}} | \hat{\Theta}_{12} | \check{\mathcal{I}} \rangle \\ &:= \langle \check{\mathcal{I}} | \left(\pi - \arccos \left(\frac{\vec{J}_1 \cdot \vec{J}_2}{\sqrt{\vec{J}_1 \cdot \vec{J}_1} \sqrt{\vec{J}_2 \cdot \vec{J}_2}} \right) \right) | \check{\mathcal{I}} \rangle \\ &\approx \pi - \arccos(\hat{n}_1 \cdot \hat{n}_2). \end{aligned} \quad (58)$$

Finally, by following the geometric interpretation of j_0 , j_1 , j_2 , j_3 , j_4 , and $\arccos(\hat{n}_1 \cdot \hat{n}_2)$ given in Eqs. (56)–(58), one can conclude that the entanglement of coherent intertwiner $E(A|B) \approx \ln(2j_0 + 1) + E_p(A|B)$ can be controlled by the local semiclassical geometry associated to the vertex. Specifically, the term $\ln(2j_0 + 1)$ is controlled by j_0 , while one can increase j_1 , j_2 , and the angle

$\arccos(\hat{n}_1 \cdot \hat{n}_2)$ at the same time to grow $E_p(A|B)$ for fixed j_0 . In the next section, we will generalize this result to the entanglement for spin-network state.

2. Coherent intertwiner with arbitrary number of legs

Let us consider the gauge-invariant coherent intertwiner space $\mathcal{H}_v^{(j, \vec{j})} = \text{Inv}_{SU(2)}[\otimes_{I=1}^P V^{j_I} \otimes \otimes_{J=1}^Q \bar{V}^{\vec{j}_J}]$ on a $(P + Q)$ -valent vertex, in which an element is given by

$$|\mathcal{I}\rangle = \int_{SU(2)} dg \otimes_{I=1}^P g |j_I, \hat{n}_I\rangle \otimes_{J=1}^Q \langle \vec{j}_J, \hat{n}_J | g^{-1}. \quad (59)$$

Similar to the coherent intertwiner with four legs, the coherent intertwiner with arbitrary number of legs can be expanded by the orthogonal recoupling basis of intertwiner space, which reads

$$\begin{aligned}
|\mathcal{I}\rangle &= \sum_j (2j+1) \left(\sum_{k,m=-j}^j |\mathcal{I}_P; j, m, k\rangle \langle \mathcal{I}_Q; j, m, k| \right) \\
&= \sum_j \sum_{j_1} \sum_{j_2} \dots \sum_{j_p} \sum_{\tilde{j}_1} \sum_{\tilde{j}_2} \dots \sum_{\tilde{j}_q} (2j+1)^{-1} \cdot c_{j,j_i,\tilde{j}_i}^{\mathcal{I}_P,\mathcal{I}_Q} \\
&\quad \cdot \sum_k \sum_{k_1,\dots,k_p} \sum_{\tilde{k}_1,\dots,\tilde{k}_q} (|j_P, j_{P-1}; j_{i_p}, k_{i_p}\rangle \otimes |j_{i_p}, k_{i_p}; j_P; j_{i_{p-1}}, k_{i_{p-1}}\rangle \otimes \dots \\
&\quad \otimes |j_2, k_2; j_2; j_1, k_1\rangle \otimes |j_1, k_1; j_1; j, k\rangle \langle \tilde{j}_Q, \tilde{j}_{Q-1}; \tilde{j}_{i_q}, \tilde{k}_{i_q}| \otimes \langle \tilde{j}_{i_q}, \tilde{k}_{i_q}; \tilde{j}_q; \tilde{j}_{i_{q-1}}, \tilde{k}_{i_{q-1}}| \otimes \dots \\
&\quad \otimes \langle \tilde{j}_2, \tilde{k}_2; \tilde{j}_2; \tilde{j}_1, \tilde{k}_1| \otimes \langle \tilde{j}_1, \tilde{k}_1; \tilde{j}_1; j, k|), \tag{60}
\end{aligned}$$

where $|j', j''; j, k\rangle := \sum_{m', m''} C_{m' m'' k}^{j' j'' j} |j', m'\rangle \otimes |j'', m''\rangle$, $|j', k'; j'', j, k\rangle := \sum_{m''} C_{k' m'' k}^{j' j'' j} |j'', m''\rangle$, and $c_{j,j_i,\tilde{j}_i}^{\mathcal{I}_P,\mathcal{I}_Q}$ is the coefficient of this expansion; see the details in the Appendix.

Now, the density matrix of the coherent intertwiner $|\mathcal{I}\rangle$ can be given by $\rho_{\mathcal{I}} \equiv \frac{|\mathcal{I}\rangle\langle\mathcal{I}|}{\langle\mathcal{I}|\mathcal{I}\rangle}$. Let us define $\mathcal{H}_A := \otimes_{i=1}^P V^{j_i}$ and $\mathcal{H}_B := \otimes_{j=1}^Q \tilde{V}^{\tilde{j}_j}$. Then, the entanglement $E(A|B)$ between A and B can be given by the von Neumann entropy of the reduced density matrices ρ_A , which are defined as

$$\rho_A := \text{Tr}_B(\rho_{\mathcal{I}}), \quad E(A|B) := -\text{Tr}_A(\rho_A \ln \rho_A). \tag{61}$$

More explicitly, ρ_A can be calculated as

$$\rho_A = \text{Tr}_B(\rho_{\mathcal{I}}) = \frac{\text{Tr}_B(|\mathcal{I}\rangle\langle\mathcal{I}|)}{\langle\mathcal{I}|\mathcal{I}\rangle}, \tag{62}$$

where

$$\langle\mathcal{I}|\mathcal{I}\rangle = \sum_j \sum_{j_1, j_2, \dots, j_p} \sum_{\tilde{j}_1, \tilde{j}_2, \dots, \tilde{j}_q} (2j+1)^{-1} c_{j,j_i,\tilde{j}_i}^{\mathcal{I}_P,\mathcal{I}_Q} \overline{c_{j,j_i,\tilde{j}_i}^{\mathcal{I}_P,\mathcal{I}_Q}}. \tag{63}$$

and

$$\text{Tr}_B(|\mathcal{I}\rangle\langle\mathcal{I}|) = \sum_j \sum_{j_1, j_2, \dots, j_p} \sum_{j'_1, j'_2, \dots, j'_p} (2j+1)^{-1} \sum_{\tilde{j}_1, \tilde{j}_2, \dots, \tilde{j}_q} c_{j,j_i,\tilde{j}_i}^{\mathcal{I}_P,\mathcal{I}_Q} \overline{c_{j,j_i,\tilde{j}_i}^{\mathcal{I}_P,\mathcal{I}_Q}} \rho_{j,j_i,\tilde{j}_i}^A, \tag{64}$$

with

$$\begin{aligned}
\rho_{j,j_i,\tilde{j}_i}^A &:= (2j+1)^{-1} \cdot \sum_k \sum_{k_1,\dots,k_p} \sum_{k'_1,\dots,k'_p} (|j_P, j_{P-1}; j_{i_p}, k_{i_p}\rangle \otimes |j_{i_p}, k_{i_p}; j_P; j_{i_{p-1}}, k_{i_{p-1}}\rangle \otimes \dots \\
&\quad \otimes |j_2, k_2; j_2; j_1, k_1\rangle \otimes |j_1, k_1; j_1; j, k\rangle \langle j_P, j_{P-1}; j'_{i_p}, k'_{i_p}| \otimes \langle j'_{i_p}, k'_{i_p}; j_P; j'_{i_{p-1}}, k'_{i_{p-1}}| \otimes \dots \\
&\quad \otimes \langle j'_2, k'_2; j_2; j'_1, k'_1| \otimes \langle j'_1, k'_1; j_1; j, k|). \tag{65}
\end{aligned}$$

It is direct to calculate that the von Neumann entropy of $\rho_{j,j_i,\tilde{j}_i}^A$, which leads to

$$S_j^A := -\text{Tr}_A(\rho_{j,j_i,\tilde{j}_i}^A \ln \rho_{j,j_i,\tilde{j}_i}^A) = \ln(2j+1). \tag{66}$$

Further, let us define

$$P_{j,j_i,j'_i} := \frac{(2j+1)^{-1} \sum_{\tilde{j}_1, \tilde{j}_2, \dots, \tilde{j}_q} c_{j,j_i,\tilde{j}_i}^{\mathcal{I}_P,\mathcal{I}_Q} \overline{c_{j,j_i,\tilde{j}_i}^{\mathcal{I}_P,\mathcal{I}_Q}}}{\langle\mathcal{I}|\mathcal{I}\rangle}, \tag{67}$$

$$\tilde{p}_j := \sum_{j_1, j_2, \dots, j_p} \sum_{j'_1, j'_2, \dots, j'_p} P_{j,j_i,j'_i}, \tag{68}$$

and

$$\bar{p}_{j,j_i,\tilde{j}_i} := \frac{p_{j,j_i,\tilde{j}_i}}{\tilde{p}_j}. \quad (69)$$

Then, the entanglement entropy $E(A|B)$ can be given by

$$E(A|B) = -\text{Tr}_A(\rho_A \ln \rho_A) = E_p(A|B) + \sum_j \tilde{p}_j \ln(2j+1), \quad (70)$$

where

$$\begin{aligned} E_p(A|B) &:= -\sum_j \sum_{j_1, j_2, \dots, j_p} \sum_{\tilde{j}_1, \tilde{j}_2, \dots, \tilde{j}_p} (p_{j,j_i,\tilde{j}_i} \ln p_{j,j_i,\tilde{j}_i}) \\ &= -\sum_j \tilde{p}_j \ln \tilde{p}_j + \sum_j \tilde{p}_j E_{\tilde{p}_j}(A|B) \end{aligned} \quad (71)$$

with

$$\begin{aligned} j_{i_p} &= |j_p \hat{n}_p + j_{p-1} \hat{n}_{p-1}|, & j_{i_{p-1}} &= |j_p \hat{n}_p + j_{p-1} \hat{n}_{p-1} + j_p \hat{n}_p|, \\ &\dots, \\ j_{i_1} &= |j_p \hat{n}_p + j_{p-1} \hat{n}_{p-1} + j_p \hat{n}_p + \dots + j_2 \hat{n}_2|, & j &= |j_p \hat{n}_p + j_{p-1} \hat{n}_{p-1} + j_p \hat{n}_p + \dots + j_1 \hat{n}_1|, \\ \tilde{j}_{i_q} &= |\tilde{j}_q \hat{n}_q + \tilde{j}_{q-1} \hat{n}_{q-1}|, & \tilde{j}_{i_{q-1}} &= |\tilde{j}_q \hat{n}_q + \tilde{j}_{q-1} \hat{n}_{q-1} + \tilde{j}_q \hat{n}_q|, \\ &\dots, \\ \tilde{j}_{i_1} &= |\tilde{j}_q \hat{n}_q + \tilde{j}_{q-1} \hat{n}_{q-1} + \tilde{j}_q \hat{n}_q + \dots + \tilde{j}_2 \hat{n}_2|, & j &= |\tilde{j}_q \hat{n}_q + \tilde{j}_{q-1} \hat{n}_{q-1} + \tilde{j}_q \hat{n}_q + \dots + \tilde{j}_1 \hat{n}_1|. \end{aligned} \quad (73)$$

This argument could be checked by evaluating the specific property of the distribution p_{j,j_i,\tilde{j}_i} . However, one can see that the general expression of p_{j,j_i,\tilde{j}_i} is too complicated to proceed with the analytical study. One may also expect a numerical calculation of the distribution p_{j,j_i,\tilde{j}_i} , and we would like to leave this to future research.

IV. ENTANGLEMENT ENTROPY OF SPIN NETWORKS

As mentioned in the Introduction, the entanglement of a spin-network basis state (3) is the composition of the entanglement carried by the intertwiners on the boundary which cuts the spin network into two parts. However, the previous computations only involve the case in which only edges of the network puncture the boundary. In this section, let us consider the case in which the network punctures the boundary at the vertices of the network, with these vertices being labeled by the gauge-invariant coherent intertwiner, which gives the expectation values of the area and face-angle operators with minimized uncertainty. Then,

$$E_{\tilde{p}_j}(A|B) := -\sum_{j_1, j_2, \dots, j_p} \sum_{\tilde{j}_1, \tilde{j}_2, \dots, \tilde{j}_p} (\bar{p}_{j,j_i,\tilde{j}_i} \ln \bar{p}_{j,j_i,\tilde{j}_i}). \quad (72)$$

It is worth it to have a discussion on this result. First, one can notice that $E(A|B)$ contains three terms $\sum_j \tilde{p}_j E_{\tilde{p}_j}(A|B)$, $\sum_j \tilde{p}_j \ln(2j+1)$, and $-\sum_j \tilde{p}_j \ln \tilde{p}_j$. This result takes the same formulation as the result (36) for the boundary entanglement of two entangled intertwiners. In fact, the recoupling edge labeled by spin j separates the coherent intertwiner as two entangled intertwiners, and the corresponding boundary entanglement of these two entangled intertwiners is given by $E(A|B)$ exactly, with $E_p(A|B)$ being the intertwiner entanglement and \tilde{p}_j being the probability distribution of the spin j on the recoupling edge. Second, it is easy to see that the entanglement entropy $E(A|B)$ depends on the distribution $p_{j,j_i,\tilde{j}_i} = \tilde{p}_j \cdot \bar{p}_{j,j_i,\tilde{j}_i}$ on the spins of the recoupling edges. In fact, by considering the peakedness property of coherent intertwiner, one can argue that p_{j,j_i,\tilde{j}_i} is peaked near the values

we will apply the results for coherent intertwiner given in previous sections to the entanglement entropy for spin networks.

For a given closed graph Γ cut by a boundary \mathcal{B} into Γ_a and Γ_b , consider a normalized and gauge-invariant spin-network state Ψ_Γ with fixed edge spins, which is given by

$$|\Psi_\Gamma\rangle = \sum_{\vec{A}, \vec{B}} \bigotimes_{c=1}^P \langle B_c | \mathcal{I}_c | A_c \rangle \cdot |\Psi_{\Gamma_a}, A_c\rangle \otimes |\Psi_{\Gamma_b}, B_c\rangle, \quad (74)$$

where Γ intersects \mathcal{B} at the punctures labeled by c with P being the numbers of punctures, \mathcal{I}_c is the normalized and gauge-invariant intertwiner on the puncture c , $\vec{A} = (A_1, \dots, A_c, \dots, A_P)$, $\vec{B} = (B_1, \dots, B_c, \dots, B_P)$, the set of $|B_c\rangle \langle A_c|$ forms an orthonormal basis of the intertwiner space $\mathcal{H}_c \ni \mathcal{I}_c$, and $|\Psi_{\Gamma_a}, A_c\rangle$ and $|\Psi_{\Gamma_b}, B_c\rangle$ correspond to the side spin networks $\langle A_c | \Psi_{\Gamma_a} \rangle$ and $\langle \Psi_{\Gamma_b} | B_c \rangle$, respectively. The entanglement $E(\Gamma_a | \Gamma_b)$ of Ψ_Γ between the two sides of the boundary is given by the von Neumann entropy of the reduce matrix

$$\rho_{\Gamma_a} := \text{Tr}_{\Gamma_b}(|\Psi_{\Gamma}\rangle\langle\Psi_{\Gamma}|) = \sum_{\vec{A}, \vec{A}', \vec{B}}^P \bigotimes_{c=1}^P \langle B_c | \mathcal{I}_c | A_c \rangle \cdot \overline{\langle A'_c | \mathcal{I}_c | B_c \rangle} \cdot |\Psi_{\Gamma_a}, A_c\rangle\langle\Psi_{\Gamma_a}, A'_c|, \quad (75)$$

which reads

$$E(\Gamma_a | \Gamma_b) := -\text{Tr}_{\Gamma_a}(\rho_{\Gamma_a} \ln \rho_{\Gamma_a}) = \sum_{c=1}^P E(A_c | B_c), \quad (76)$$

where $E(A_c | B_c) := -\text{Tr}_{A_c}(\rho_{A_c} \ln \rho_{A_c})$ with

$$\rho_{A_c} := \text{Tr}_{B_c}(|\mathcal{I}_c\rangle\langle\mathcal{I}_c|) = \sum_{A_c, A'_c, B_c} \langle B_c | \mathcal{I}_c | A_c \rangle \cdot \overline{\langle A'_c | \mathcal{I}_c | B_c \rangle} \cdot |A_c\rangle\langle A'_c|. \quad (77)$$

Equation (76) shows that, for the spin-network state Ψ_{Γ} which allows the decomposition (74), the entanglement $E(\Gamma_a | \Gamma_b)$ between the spin networks inside and outside a boundary is the sum of the entanglement $E(A_c | B_c)$ carried by the intertwiners \mathcal{I}_c on this boundary. By recalling Theorem 2 given in Sec. III A, the entanglement $E(\Gamma_a | \Gamma_b)$ of the spin network can be further written as

$$E(\Gamma_a | \Gamma_b) = \sum_{c=1}^P \left(\sum_{j_c} \tilde{p}_{j_c} \ln(2j_c + 1) - \sum_{j_c} \tilde{p}_{j_c} \ln \tilde{p}_{j_c} + \sum_{j_c} \tilde{p}_{j_c} E_{j_c}(v_1^c | v_2^c) \right), \quad (78)$$

wherein the intertwiner \mathcal{I}_c is cut as two parts v_1^c and v_2^c which are linked by a internal edge labeled by j_c as shown in Fig. 1, with \tilde{p}_{j_c} being the probability distribution of j_c and $E_{j_c}(v_1^c | v_2^c)$ being the entanglement between v_1^c and v_2^c . Especially, for the case in which only 2-valents vertices appear on the boundary \mathcal{B} , which means that \mathcal{B} is only punctured by edges of Γ , the entropy given by Eq. (78) reduces to $E(\Gamma_a | \Gamma_b) = \sum_{c=1}^P \ln(2j_c + 1)$ as shown in Refs. [51,53].

It is also worth it to consider the case in which the vertices on the boundary are labeled by the coherent intertwiners, which ensures that the boundary has a fixed expectation value of area with minimal uncertainty. Let us focus on the case in which all the punctures on the boundary are given by 4-valents vertices of graph Γ , with two legs being inside the boundary and the other two legs outside the boundary for each 4-valents vertex as shown in Fig. 11. Then, the entanglement $E(\Gamma_a | \Gamma_b)$ of the spin network is given by

$$E(\Gamma_a | \Gamma_b) = \sum_{c=1}^P \left(\sum_{j_c} p_{j_c} \ln(2j_c + 1) - \sum_{j_c} p_{j_c} \ln p_{j_c} \right) \quad (79)$$

based on Eq. (55), wherein each coherent intertwiner on the 4-valents vertex is cut as two parts linked by an internal edge

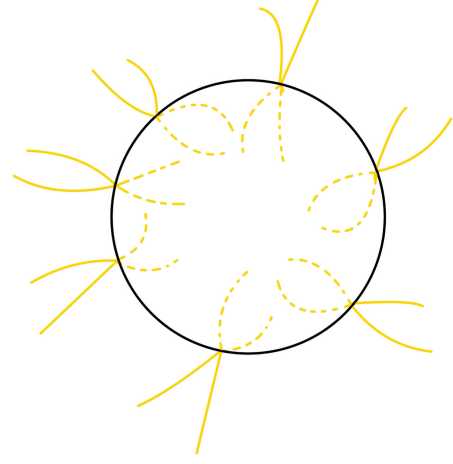


FIG. 11. All the punctures on the boundary are given by 4-valents vertices of graph Γ , with two legs being inside the boundary and the other two legs outside the boundary for each 4-valents vertex.

labeled by j_c as shown in Fig. 7, with \tilde{p}_{j_c} being the probability distribution of j_c .

Now, let us adapt our discussion to the special case $j_1^c = j_2^c = j_3^c = j_4^c$ which has been considered in our numerical simulation. Then, one has $\sum_{j_c} p_{j_c} \ln(2j_c + 1) \approx \ln(2j_0^c + 1)$, with $j_0^c := |j_1^c \hat{n}_1^c + j_2^c \hat{n}_2^c| = j_1 \sqrt{2 + 2\hat{n}_1 \cdot \hat{n}_2} \approx \sum_{j_c} j_c p_{j_c}$ controlling the contribution of the coherent intertwiner on puncture c to the area of the boundary \mathcal{B} . More explicitly, one has the entanglement

$$E(\Gamma_a | \Gamma_b) \approx \sum_{c=1}^P \left(\ln(2j_0^c + 1) - \sum_{j_c} p_{j_c} \ln p_{j_c} \right) \quad (80)$$

and the expectation value of the area of boundary \mathcal{B} ,

$$\text{Ar}(\mathcal{B}) = \langle \Psi_{\Gamma} | \widehat{\text{Ar}}(\mathcal{B}) | \Psi_{\Gamma} \rangle \approx 8\pi\beta\ell_{\text{pl}}^2 \sum_{c=1}^P j_0^c, \quad (81)$$

by using Eq. (56). Let us fix $\text{Ar}(\mathcal{B})$ and suppose that all punctures c given by 4-valents vertices are labeled by the same coherent intertwiner; then, one has $E(\Gamma_a | \Gamma_b) = P \cdot (\ln(2j_0^c + 1) - \sum_{j_c} p_{j_c} \ln p_{j_c})$ and $\text{Ar}(\mathcal{B}) \approx 8\pi\beta\ell_{\text{pl}}^2 j_0^c \cdot P$, which lead to

$$E(\Gamma_a | \Gamma_b) \approx \frac{\text{Ar}(\mathcal{B}) (\ln(2j_0^c + 1) - \sum_{j_c} p_{j_c} \ln p_{j_c})}{4\ell_{\text{pl}}^2} = \frac{\text{Ar}(\mathcal{B}) \beta_c}{4\ell_{\text{pl}}^2 \beta}, \quad (82)$$

where we defined

$$\beta_c := \frac{\ln(2j_0^c + 1)}{2\pi j_0^c} - \frac{\sum_{j_c} p_{j_c} \ln p_{j_c}}{2\pi j_0^c}. \quad (83)$$

Let us analyze that the parameter β_c determined by Eq. (83) can be controlled by $j_0^c = j_1^c \sqrt{2 + 2\hat{n}_1^c \cdot \hat{n}_2^c}$ and $-\sum_{j_c} p_{j_c} \ln p_{j_c}$ independently. First, for fixed $\hat{n}_1^c \cdot \hat{n}_2^c$, one can notice that β_c decreases with j_1^c going large by using Table III; then, for fixed $j_0^c = j_1^c \sqrt{2 + 2\hat{n}_1^c \cdot \hat{n}_2^c}$, the term $-\sum_{j_c} p_{j_c} \ln p_{j_c}$ can be controlled by j_1^c and $\hat{n}_1^c \cdot \hat{n}_2^c$ following the results in Sec. III C 1. Thus, β_c can be controlled by j_1^c and $\arccos(\hat{n}_1^c \cdot \hat{n}_2^c)$, which describes the semiclassical geometry of the polyhedra related to the coherent intertwiner. One may use some conditions for horizon to constrain β_c , to achieve a specific correction to the Bekenstein-Hawking formula.

Finally, we can conclude that, for the spin network puncturing a boundary by its vertices labeled by coherent intertwiners, the entanglement entropy of such spin-network state is not only determined by the area of the boundary but also carries a quantum correction controlled by the semiclassical geometry associated to the vertices on the boundary.

V. CONCLUSION

The entanglements carried by the specific intertwiners and spin networks are studied in previous sections. We first review the relation between the boundary entanglement and intertwiner entanglement and extend the result to the case that the internal edge carries a spin superposition. Then, we turn to consider the specific intertwiners on a four-valents vertex, which is decomposed as two parts A and B attached by the labels $(j_1 m_1, j_2 m_2)$ and $(j_3 m_3, j_4 m_4)$, respectively. By introducing the group averaging to the tensor-product-type intertwiner on the four-valents vertex, we calculate the entanglement entropy $E(A|B)$ encoded in the group-averaged tensor-product intertwiner with various weights. The results show that, for the group-averaged tensor-product intertwiner with highest (and lowest) weight, the entanglement entropy is able to capture the main character of the probability distribution p_j of the recoupling spin j . This result suggests considering the entanglement entropy encoded in the gauge-invariant coherent intertwiners.

To compute the entanglement for coherent intertwiner, we introduce the recoupling edges to decompose the coherent intertwiner labeled by $(j_1 \hat{n}_1, j_2 \hat{n}_2)$ and $(j_3 \hat{n}_3, j_4 \hat{n}_4)$. We find that the entanglement for the coherent intertwiner is determined by the probability distribution p_j of the spins j on the recoupling edges of the coherent intertwiner, and the result of entanglement $E(A|B)$ is composed by the sum of two terms $E_p(A|B)$ and $E_0(A|B)$. The first term $E_p(A|B)$ is just the Shannon entropy of the distribution p_j , while the second term $E_0(A|B)$ is the expectation value of $\ln(2j+1)$ with respect to the distribution p_j . Our results show that p_j has a peak near $j = j_0 \equiv |j_1 \hat{n}_1 + j_2 \hat{n}_2|$, which leads to $E_0(A|B) = \sum_j p_j S_j^A \approx \ln(2j_0 + 1)$; especially, this peak shrinks relative to the range of j with the boundary spins j_1, j_2, j_3, j_4 getting

larger, and it also shrink with the angle $\arccos(\hat{n}_1 \cdot \hat{n}_2)$ decreasing. Thus, we find that $E_p(A|B)$ increases with the angle $\arccos(\hat{n}_1 \cdot \hat{n}_2)$ getting larger, and the two terms $E_0(A|B)$ and $E_p(A|B)$ both increase no more than logarithmic growth with j_1, j_2, j_3, j_4 going large. Besides, we also explain the geometric interpretation of j_0, j_1, j_2, j_3, j_4 and $\arccos(\hat{n}_1 \cdot \hat{n}_2)$, and then we analyze that the entanglement of coherent intertwiner $E(A|B) \approx \ln(2j_0 + 1) + E_p(A|B)$ can be controlled by the local semiclassical geometry associated to the vertex.

We further extend the analytical calculation part of entanglement to the case of gauge-invariant coherent intertwiner on a $(P+Q)$ -valents vertex, which is also separated as two parts A and B attached by $(j_1, \hat{n}_1, j_2, \hat{n}_2, \dots, j_P, \hat{n}_P)$ and $(\tilde{j}_1, \hat{n}_1, \tilde{j}_2, \hat{n}_2, \dots, \tilde{j}_Q, \hat{n}_Q)$, respectively. By introducing the recoupling edges to decompose the gauge-invariant coherent intertwiner, we give the probability distribution p_{j, \tilde{j}_i} of the spins j, \tilde{j}_i on the recoupling edges analytically and show that the entanglement between A and B is determined by p_{j, \tilde{j}_i} .

Moreover, we apply the previous results for coherent intertwiner to the entanglement of spin networks. Specifically, we consider the spin network puncturing a boundary by its vertices labeled by coherent intertwiners and fix the expectation value of area of the boundary. Our results show that the entanglement of such spin-network state can be evaluated by $E(\Gamma_a | \Gamma_b) \approx \frac{\text{Ar}(\mathcal{B}) \beta_c}{4\ell_{\text{pl}}^2 \beta}$ in some specific cases, where $\text{Ar}(\mathcal{B})$ is the area of the boundary and $\beta_c := \frac{\ln(2j_0^c + 1)}{2\pi j_0^c} - \frac{\sum_{j_c} p_{j_c} \ln p_{j_c}}{2\pi j_0^c}$ is controlled by j_0^c and p_{j_c} , which are related to the local semiclassical geometries described by the coherent intertwiners. Thus, we can conclude that the entanglement of spin networks is not only determined by the area of the boundary but also carries a quantum correction controlled by the semiclassical geometry associated to the vertices on the boundary. In fact, the entanglement for the quantum state of geometry in the framework of LQG is also involved in the previous literature [35–50], wherein the research accounts for entanglement between bulk and boundary (i.e., isolated horizon) quantum spacetime states. The difference between the previous and present works can be phrased as the previous literature being about entanglement between spin-network states and the present paper being about entanglement between semiclassical (coherent) states.

It is worth it to have some discussion on these results. First, one should notice that the entanglement entropy $E(A|B)$ is given based on the gauge-invariant coherent intertwiners, which belong to the gauge-invariant subspace of the total system $\mathcal{H}_A \otimes \mathcal{H}_B$. Thus, $E(A|B)$ describes the entanglement between some gauge-invariant degrees of freedom, e.g., the face-angle $\pi - \arccos \hat{n}_1 \cdot \hat{n}_2$. Nevertheless, the appearance of the factor $\ln(2j+1)$ comes from breaking the $SU(2)$ gauge invariance, and

the physical meaning of the factor $\ln(2j+1)$ depends on how to define boundaries at the quantum level for non-Abelian lattice gauge theories and LQG [57]. Different than the $SU(2)$ gauge breaking at the quantum level in the present paper, the classical gauge-fixing scheme is used to treat the gauge degrees of freedom on the inner boundary in several previous works [35,45], and it may suggest us a new treatment of the quantum gauge breaking.

Second, the entanglement between the legs of coherent intertwiner is related to the face angle of the semiclassical polyhedron. Recall that p_j has a peak near $j_0 \equiv |j_1 \hat{n}_1 + j_2 \hat{n}_2|$ and this peak shrinks with the angle $\arccos(\hat{n}_1 \cdot \hat{n}_2)$ decreasing. Thus, the Shannon entropy $E_p(A|B)$ of the distribution p_j decreases with the face angle $\pi - \arccos(\hat{n}_1 \cdot \hat{n}_2)$ increasing. Nevertheless, one also notes that another term $E_0(A|B) \approx \ln(2j_0 + 1)$ in $E(A|B)$ increases with the face angle $\pi - \arccos(\hat{n}_1 \cdot \hat{n}_2)$ increasing. Hence, the entanglement $E(A|B)$ may not have monotonous dependency on the face angle $\pi - \arccos(\hat{n}_1 \cdot \hat{n}_2)$; e.g., as shown in Table IV, $E(A|B)$ increases first and then decreases with the face angle $\pi - \arccos(\hat{n}_1 \cdot \hat{n}_2)$ increasing for $j_1 = j_2 = j_3 = j_4 = 20$.

Third, as we shown in Sec. III A, we would like to emphasize that the entanglement on the 2-vertex graph with one link is independent on holonomy insertion [57]. In other words, the holonomy living along the edge connecting these two vertices is irrelevant to the entanglement entropy altogether. This property is attributed to the observation that the holonomy can be eliminated by a boundary unitary. This implies that the entanglement does not distinguish between a 2-vertex graph and its coarse-grained graph (single vertex) provided that there is only one link. For the cases of two-vertices graph with multilinks, the nontrivial loop is introduced, which should be viewed as excitation of gauge curvature [64,65] or interpreted as topological defect [66–68]. The related studies of entanglement for the cases can be found in Refs. [68,69].

Moreover, these results maybe also generalized to more complicated coarse-grained models [51,54,55,57,69–72].

Finally, by combining the results in present paper and that in previous works [40,45], one can conclude that the black hole entropy is now predicted to be the logarithmic corrections to the Bekenstein-Hawking area law, plus an additional correction contribution arising from the semiclassical (coherent) states. Notice that the correction arising from the semiclassical (coherent) states contains the undetermined Barbero-Immirzi parameter β , which implies that the LQG has certain inherent incompleteness. Besides, the correction arising from the semiclassical (coherent) states also relies on the local semiclassical geometries on the boundary, which may be fixed (or restricted) by introducing some boundary conditions or considering (semiclassical) dynamics of LQG. We would like to leave this to future research.

ACKNOWLEDGMENTS

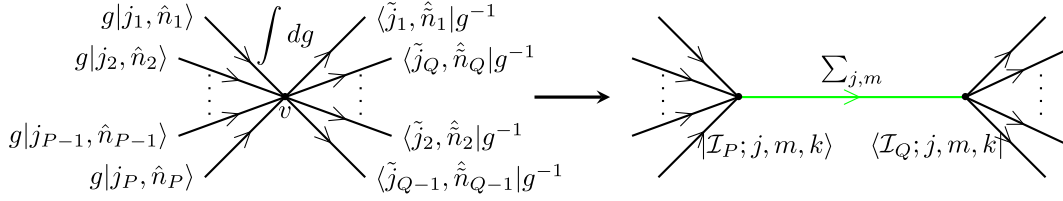
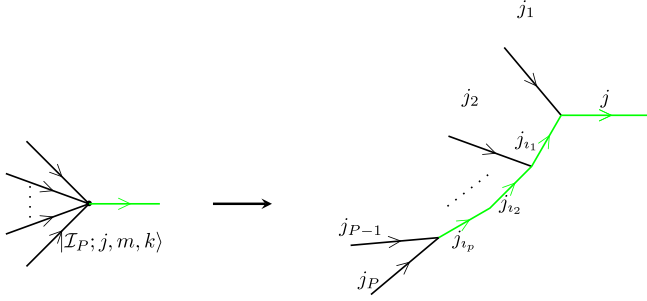
This work is supported by the project funded by the National Natural Science Foundation of China (NSFC) with Grants No. 12405062 and No. 12165005. G. L. is supported by the Fundamental Research Funds for the Central Universities with Grant No. 21624340, and the Science and Technology Planning Project of Guangzhou with Grant No. 2024A04J4030. Q. C. is funded within the QuantERA II Programme that has received funding from the European Union's Horizon 2020 research and innovation programme under Grant Agreement No. 101017733 (VERIQ-TAS).

APPENDIX: RECOUPLING EXPANSION OF COHERENT INTERTWINER WITH ARBITRARY NUMBER OF LEGS

By introduce a recoupling edge labeled by spin j , the coherent intertwiner $|\mathcal{I}\rangle$ can be decomposed as

$$\begin{aligned}
|\mathcal{I}\rangle &= \int_{SU(2)} dg \bigotimes_{I=1}^P g|j_I, \hat{n}_I\rangle \int_{SU(2)} dh \delta(g^{-1}h) \bigotimes_{J=1}^Q \langle \tilde{j}_J, \hat{n}_J | h^{-1} \\
&= \sum_j (2j+1) \int_{SU(2)} dg \int_{SU(2)} dh \bigotimes_{I=1}^P g|j_I, \hat{n}_I\rangle \text{tr}^j(g^{-1}h) \bigotimes_{J=1}^Q \langle \tilde{j}_J, \hat{n}_J | h^{-1} \\
&= \sum_j (2j+1) \left(\sum_{m,k=-j}^j \int_{SU(2)} dg \bigotimes_{I=1}^P g|j_I, \hat{n}_I\rangle \otimes \langle j, m | g^{-1} | j, k \rangle \otimes \int_{SU(2)} dh \langle j, k | h | j, m \rangle \bigotimes_{J=1}^Q \langle \tilde{j}_J, \hat{n}_J | h^{-1} \right) \\
&= \sum_j (2j+1) \left(\sum_{m,k=-j}^j |\mathcal{I}_P; j, m, k\rangle \langle \mathcal{I}_Q; j, m, k| \right), \tag{A1}
\end{aligned}$$

where


 FIG. 12. The illustration of recoupling spin j for \mathcal{I} .

 FIG. 13. The illustration of recoupling spins for $|\mathcal{I}_P; j, m, k\rangle$.

$$|\mathcal{I}_P; j, m, k\rangle := \int_{SU(2)} dg \bigotimes_{I=1}^P g|j_I, \hat{n}_I\rangle \otimes \langle j, m|g^{-1}|j, k\rangle,$$

$$\langle \mathcal{I}_Q; j, m, k| := \int_{SU(2)} dh \langle j, k|h|j, m\rangle \bigotimes_{J=1}^Q \langle \tilde{j}_J, \hat{n}_J|h^{-1} \quad (\text{A2})$$

are projectors that send tensor representations to recoupling representations; see the illustration in Fig. 12.

One can further insert recoupling edges adapting to a recoupling scheme for $|\mathcal{I}_P, j, m\rangle$ step by step. Following the recoupling scheme illustrated in Fig. 13 and using character formula for delta function

$$g|jm\rangle \otimes \langle j'm'|g^{-1}$$

$$= \int_{SU(2)} dh \delta(g^{-1}h) h|jm\rangle \otimes \langle j'm'|h^{-1}$$

$$= \sum_{j''} (2j'' + 1) \int_{SU(2)} dh \text{tr}^{j''} (hg^{-1}) h|jm\rangle \otimes \langle j'm'|h^{-1},$$

one can get

$$|\mathcal{I}_P; j, m, k\rangle := \int_{SU(2)} dg \left(\bigotimes_{I=1}^P g|j_I, \hat{n}_I\rangle \right) \otimes \langle j, m|g^{-1}|j, k\rangle$$

$$= \sum_{j_1} (2j_1 + 1) \sum_{m_1, k_1 = -j_1}^{j_1} \int_{SU(2)} dg \bigotimes_{I=2}^P g|j_I, \hat{n}_I\rangle \cdot \langle j_1, m_1|g^{-1}|j_1, k_1\rangle \otimes |j_1, k_1, m_1, j_1, \hat{n}_1, jmk\rangle$$

$$= \sum_{j_1} \sum_{j_2} (2j_1 + 1)(2j_2 + 1) \left(\sum_{m_1, k_1 = -j_1}^{j_1} \sum_{m_2, k_2 = -j_2}^{j_2} \int_{SU(2)} dg \bigotimes_{I=3}^P g|j_I, \hat{n}_I\rangle \cdot \langle j_2, m_2|g^{-1}|j_2, k_2\rangle \right.$$

$$\left. \otimes |j_2, k_2, m_2, j_2, \hat{n}_2, j_1, m_1, k_1\rangle \otimes |j_1, k_1, m_1, j_1, \hat{n}_1, jmk\rangle \right)$$

$$= \sum_{j_1} \sum_{j_2} \dots \sum_{j_p} (2j_1 + 1)(2j_2 + 1) \dots (2j_p + 1) \cdot \left(\sum_{m_1, k_1 = -j_1}^{j_1} \sum_{m_2, k_2 = -j_2}^{j_2} \dots \sum_{m_p, k_p = -j_p}^{j_p} |j_P \hat{n}_P, j_{P-1} \hat{n}_{P-1}, j_p, m_p, k_p\rangle \right.$$

$$\left. \otimes |j_p, k_p, m_p, j_p, \hat{n}_p, j_{p-1}, m_{p-1}, k_{p-1}\rangle \otimes \dots \otimes |j_2, k_2, m_2, j_2, \hat{n}_2, j_1, m_1, k_1\rangle \otimes |j_1, k_1, m_1, j_1, \hat{n}_1, jmk\rangle \right)$$

$$= \sum_{j_1} \sum_{j_2} \dots \sum_{j_p} (2j + 1)^{-1} \cdot \sum_{m_1, k_1 = -j_1}^{j_1} \sum_{m_2, k_2 = -j_2}^{j_2} \dots \sum_{m_p, k_p = -j_p}^{j_p} c_{\hat{n}_P, \hat{n}_{P-1}, m_p}^{j_P, j_{P-1}, j_p} c_{m_p, \hat{n}_p, m_{p-1}}^{j_p, j_p, j_{p-1}} \dots c_{m_2, \hat{n}_2, m_1}^{j_2, j_2, j_1} c_{m_1, \hat{n}_1, m}^{j_1, j_1, j}$$

$$\cdot (|j_P, j_{P-1}; j_p, k_p\rangle \otimes |j_p, k_p; j_p; j_{p-1}, k_{p-1}\rangle \otimes \dots \otimes |j_2, k_2; j_2; j_1, k_1\rangle \otimes |j_1, k_1; j_1; j, k\rangle) \quad (\text{A3})$$

with $p := P - 2$, where we defined

$$c_{m_1, \hat{n}_1, m}^{j_1, j_1, j} := \sum_{k'_1 = -j_1}^{j_1} \sum_{k' = -j}^j \langle j_1, k'_1; j_1; j, k' | j_1, k'_1, m_1, j_1 \hat{n}_1, j, k \rangle, \quad (\text{A4})$$

$$c_{m_2, \hat{n}_2, m_1}^{j_2, j_2, j_1} := \sum_{k'_2 = -j_2}^{j_2} \sum_{k'_1 = -j_1}^{j_1} \langle j_2, k'_2; j_2; j_1, k'_1 | j_2, k'_2, m_2, j_2 \hat{n}_2, j_1, m_1, k'_1 \rangle, \quad (\text{A5})$$

$$\dots, \quad (\text{A6})$$

$$c_{\hat{n}_p, \hat{n}_{p-1}, m_p}^{j_p, j_{p-1}, j_{1p}} := \sum_{k'_{1p} = -j_{1p}}^{j_{1p}} \langle j_p, j_{p-1}; j_{1p}, k'_{1p} | j_p \hat{n}_p, j_{p-1} \hat{n}_{p-1}, j_{1p}, m_p, k'_{1p} \rangle, \quad (\text{A7})$$

and

$$|j_1, k'_1, m_1, j_1 \hat{n}_1, j, k \rangle := \int_{SU(2)} dg g |j_1, \hat{n}_1 \rangle \langle j_1, k'_1 | g |j_1, m_1 \rangle \cdot \langle j, m | g^{-1} |j, k \rangle, \quad (\text{A8})$$

$$|j_2, k'_2, m_2, j_2 \hat{n}_2, j_1, m_1, k'_1 \rangle := \int_{SU(2)} dg g |j_2, \hat{n}_2 \rangle \langle j_2, k'_2 | g |j_2, m_2 \rangle \cdot \langle j_1, m_1 | g^{-1} |j_1, k'_1 \rangle, \quad (\text{A9})$$

$$\dots, \quad (\text{A10})$$

$$|j_p \hat{n}_p, j_{p-1} \hat{n}_{p-1}, j_{1p}, m_p, k'_{1p} \rangle := \int_{SU(2)} dg g |j_p, \hat{n}_p \rangle \otimes g |j_{p-1}, \hat{n}_{p-1} \rangle \langle j_{1p}, m_p | g^{-1} |j_{1p}, k'_{1p} \rangle, \quad (\text{A11})$$

with $|j', j''; j, k \rangle := \sum_{m', m''} C_{m' m'' k}^{j' j'' j} |j', m' \rangle \otimes |j'', m'' \rangle$, $|j', k'; j'', j, k \rangle := \sum_{m''} C_{k' m'' k}^{j' j'' j} |j'', m'' \rangle$. Similarly, as the illustration in Fig. 14, one can expand

$$\begin{aligned} \langle \mathcal{I}_Q; j, m, k | &:= \int_{SU(2)} dh \langle j, k | h |j, m \rangle \bigotimes_{J=1}^Q \langle \tilde{j}_J, \hat{n}_J | h^{-1} \\ &= \sum_{\tilde{j}_1} (2\tilde{j}_1 + 1) \left(\sum_{\tilde{m}_1, \tilde{k}_1 = -\tilde{j}_1}^{\tilde{j}_1} \int_{SU(2)} dh \langle \tilde{j}_1, \tilde{k}_1 | h | \tilde{j}_1, \tilde{m}_1 \rangle \bigotimes_{J=2}^Q \langle \tilde{j}_J, \hat{n}_J | h^{-1} \otimes \langle \tilde{j}_1, \tilde{m}_1, \tilde{k}_1, \tilde{j}_1 \hat{n}_1, j, k, m | \right) \\ &= \sum_{\tilde{j}_1} \sum_{\tilde{j}_2} \dots \sum_{\tilde{j}_q} (2j + 1)^{-1} \cdot \sum_{\tilde{m}_1, \tilde{k}_1 = -\tilde{j}_1}^{\tilde{j}_1} \sum_{\tilde{m}_2, \tilde{k}_2 = -\tilde{j}_2}^{\tilde{j}_2} \dots \sum_{\tilde{m}_q, \tilde{k}_q = -\tilde{j}_q}^{\tilde{j}_q} c_{\hat{n}_Q, \hat{n}_{Q-1}, \tilde{m}_q}^{\tilde{j}_Q, \tilde{j}_{Q-1}, \tilde{j}_q} c_{\tilde{m}_q, \hat{n}_q, \tilde{m}_{q-1}}^{\tilde{j}_q, \tilde{j}_q, \tilde{j}_{q-1}} \dots c_{\tilde{m}_2, \hat{n}_2, \tilde{m}_1}^{\tilde{j}_2, \tilde{j}_2, \tilde{j}_1} c_{\tilde{m}_1, \hat{n}_1, j}^{\tilde{j}_1, \tilde{j}_1, j} \\ &\cdot (\langle \tilde{j}_Q, \tilde{j}_{Q-1}; \tilde{j}_q, \tilde{k}_q | \otimes \langle \tilde{j}_q, \tilde{k}_q; \tilde{j}_q; \tilde{j}_{q-1}, \tilde{k}_{q-1} | \otimes \dots \otimes \langle \tilde{j}_2, \tilde{k}_2; \tilde{j}_2; \tilde{j}_1, \tilde{k}_1 | \otimes \langle \tilde{j}_1, \tilde{k}_1; \tilde{j}_1; j, k |) \end{aligned} \quad (\text{A12})$$

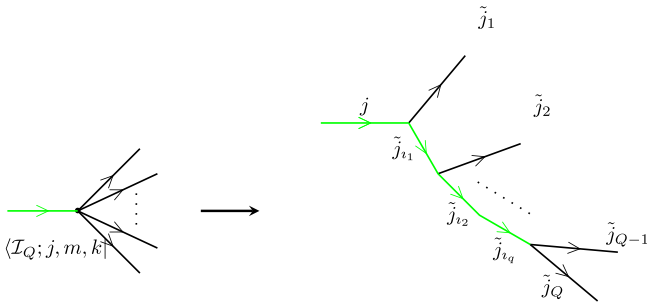


FIG. 14. The illustration of recoupling spins for $\langle \mathcal{I}_Q; j, m, k |$.

with $q = Q - 2$, where we defined

$$c_{\tilde{m}_1, \hat{n}_1, m}^{\tilde{j}_1, \tilde{j}_1, j} := \sum_{k'_1, k'} \langle \tilde{j}_1, \tilde{m}_1, \tilde{k}'_1, \tilde{j}_1 \hat{n}_1, j, k' | \tilde{j}_1, \tilde{k}'_1; \tilde{j}_1; j, k \rangle, \quad (\text{A13})$$

$$c_{\tilde{m}_2, \hat{n}_2, \tilde{m}_1}^{\tilde{j}_2, \tilde{j}_2, \tilde{j}_1} := \sum_{k'_1, k'_2} \langle \tilde{j}_2, \tilde{m}_2, \tilde{k}'_2, \tilde{j}_2 \hat{n}_2, \tilde{j}_1, \tilde{k}'_1, \tilde{m}_1 | \tilde{j}_2, \tilde{k}'_2; \tilde{j}_2; \tilde{j}_1, \tilde{k}'_1 \rangle, \quad (\text{A14})$$

$$\dots, \quad (\text{A15})$$

$$c_{\tilde{n}_Q, \tilde{n}_{Q-1}, \tilde{m}_{i_q}}^{\tilde{j}_Q, \tilde{j}_{Q-1}, \tilde{j}_{i_q}} := \sum_{\tilde{k}'_{i_q}} \langle \tilde{j}_Q \hat{n}_Q, \tilde{j}_{Q-1} \hat{n}_{Q-1}, \tilde{j}_{i_q} \tilde{k}'_{i_q} \tilde{m}_{i_q} | \tilde{j}_Q, \tilde{j}_{Q-1}; \tilde{j}_{i_q}, \tilde{k}'_{i_q} \rangle, \quad (\text{A16})$$

and

$$\langle \tilde{j}_{i_1} \tilde{m}_{i_1} \tilde{k}'_{i_1}, \tilde{j}_1 \hat{n}_1, jk'm | := \int_{SU(2)} dg \otimes \langle j, k' | g | j, m \rangle \langle \tilde{j}_{i_1}, \tilde{m}_{i_1} | g^{-1} | \tilde{j}_{i_1}, \tilde{k}'_{i_1} \rangle \otimes \langle \tilde{j}_1, \hat{n}_1 | g^{-1}, \quad (\text{A17})$$

$$\langle \tilde{j}_{i_2} \tilde{m}_{i_2} \tilde{k}'_{i_2}, \tilde{j}_2 \hat{n}_2, \tilde{j}_{i_1} \tilde{k}'_{i_1} \tilde{m}_{i_1} | := \int_{SU(2)} dg \langle \tilde{j}_{i_1}, \tilde{k}'_{i_1} | g | \tilde{j}_{i_1}, \tilde{m}_{i_1} \rangle \langle \tilde{j}_{i_2}, \tilde{m}_{i_2} | g^{-1} | \tilde{j}_{i_2}, \tilde{k}'_{i_2} \rangle \otimes \langle \tilde{j}_2, \hat{n}_2 | g^{-1}, \quad (\text{A18})$$

$$\dots, \quad (\text{A19})$$

$$\langle \tilde{j}_Q \hat{n}_Q, \tilde{j}_{Q-1} \hat{n}_{Q-1}, \tilde{j}_{i_q} \tilde{k}'_{i_q} \tilde{m}_{i_q} | := \int_{SU(2)} dg \langle \tilde{j}_{i_q}, \tilde{k}'_{i_q} | g | \tilde{j}_{i_q}, \tilde{m}_{i_q} \rangle \langle \tilde{j}_Q, \hat{n}_Q | g^{-1} \otimes \langle \tilde{j}_{Q-1}, \hat{n}_{Q-1} | g^{-1}. \quad (\text{A20})$$

Then, one has

$$\begin{aligned} |\mathcal{I}\rangle &= \sum_j (2j+1) \left(\sum_{m,k=-j}^j |\mathcal{I}_P; j, m, k\rangle \langle \mathcal{I}_Q; j, m, k| \right) \\ &= \sum_j \sum_{j_1} \sum_{j_2} \dots \sum_{j_p} \sum_{\tilde{j}_1} \sum_{\tilde{j}_2} \dots \sum_{\tilde{j}_q} (2j+1)^{-1} \\ &\quad \cdot c_{j, j_1, \tilde{j}_1}^{\mathcal{I}_P, \mathcal{I}_Q} \cdot \sum_{k=-j}^j \sum_{\tilde{k}_1=-\tilde{j}_1}^{\tilde{j}_1} \sum_{\tilde{k}_2=-\tilde{j}_2}^{\tilde{j}_2} \dots \sum_{\tilde{k}_{i_q}=-\tilde{j}_{i_q}}^{\tilde{j}_{i_q}} \sum_{k_1=-j_1}^{j_1} \sum_{k_2=-j_2}^{j_2} \dots \sum_{k_p=-j_p}^{j_p} (|j_P, j_{P-1}; j_p, k_{i_p}\rangle \\ &\quad \otimes |j_p, k_{i_p}; j_p; j_{p-1}, k_{i_{p-1}}\rangle \otimes \dots \otimes |j_2, k_{i_2}; j_2; j_1, k_{i_1}\rangle \otimes |j_1, k_{i_1}; j_1; j, k\rangle \langle \tilde{j}_Q, \tilde{j}_{Q-1}; \tilde{j}_{i_q}, \tilde{k}_{i_q}| \\ &\quad \otimes \langle \tilde{j}_{i_q}, \tilde{k}_{i_q}; \tilde{j}_q; \tilde{j}_{i_q-1}, \tilde{k}_{i_{q-1}}| \otimes \dots \otimes \langle \tilde{j}_{i_2}, \tilde{k}_{i_2}; \tilde{j}_2; \tilde{j}_{i_1}, \tilde{k}_{i_1}| \otimes \langle \tilde{j}_{i_1}, \tilde{k}_{i_1}; \tilde{j}_1; j, k|), \end{aligned} \quad (\text{A21})$$

where

$$\begin{aligned} c_{j, j_1, \tilde{j}_1}^{\mathcal{I}_P, \mathcal{I}_Q} &:= \sum_{m=-j}^j \sum_{\tilde{m}_1=-\tilde{j}_1}^{\tilde{j}_1} \sum_{\tilde{m}_2=-\tilde{j}_2}^{\tilde{j}_2} \dots \sum_{\tilde{m}_{i_q}=-\tilde{j}_{i_q}}^{\tilde{j}_{i_q}} \sum_{m_1=-j_1}^{j_1} \sum_{m_2=-j_2}^{j_2} \dots \sum_{m_p=-j_p}^{j_p} c_{\tilde{n}_Q, \tilde{n}_{Q-1}, \tilde{m}_{i_q}}^{\tilde{j}_Q, \tilde{j}_{Q-1}, \tilde{j}_{i_q}} \\ &\quad \cdot c_{\tilde{m}_{i_q}, \tilde{n}_q, \tilde{m}_{i_{q-1}}}^{\tilde{j}_{i_q}, \tilde{j}_q, \tilde{j}_{i_{q-1}}} \dots c_{\tilde{m}_{i_2}, \tilde{n}_2, \tilde{m}_{i_1}}^{\tilde{j}_{i_2}, \tilde{j}_2, \tilde{j}_{i_1}} c_{\tilde{m}_{i_1}, \tilde{n}_1, m}^{\tilde{j}_{i_1}, \tilde{j}_1, j} c_{\hat{n}_P, \hat{n}_{P-1}, m_{i_p}}^{j_P, j_{P-1}, j_{i_p}} c_{m_{i_p}, \hat{n}_p, m_{i_{p-1}}}^{j_p, j_p, j_{i_{p-1}}} \dots c_{m_{i_2}, \hat{n}_2, m_{i_1}}^{j_2, j_2, j_{i_1}} c_{m_{i_1}, \hat{n}_1, m}^{j_1, j_1, j}. \end{aligned} \quad (\text{A22})$$

- [1] A. Ashtekar and J. Pullin, *Loop Quantum Gravity: The First 30 Years* (World Scientific, Singapore, 2017).
 [2] A. Ashtekar and J. Lewandowski, Background independent quantum gravity: A status report, *Classical Quantum Gravity* **21**, R53 (2004).

- [3] T. Thiemann, *Modern Canonical Quantum General Relativity* (Cambridge University Press, Cambridge, England, 2007).
 [4] C. Rovelli and F. Vidotto, *Covariant Loop Quantum Gravity: An Elementary Introduction to Quantum Gravity*

- and *Spinfoam Theory* (Cambridge University Press, Cambridge, England, 2014).
- [5] C. Rovelli, *Quantum Gravity* (Cambridge University Press, Cambridge, England, 2007).
- [6] M. Han, M. A. Yongge, and W. Huang, Fundamental structure of loop quantum gravity, *Int. J. Mod. Phys. D* **16**, 1397 (2005).
- [7] C. Rovelli and S. Speziale, On the geometry of loop quantum gravity on a graph, *Phys. Rev. D* **82**, 044018 (2010).
- [8] L. Freidel and S. Speziale, From twistors to twisted geometries, *Phys. Rev. D* **82**, 084041 (2010).
- [9] L. Freidel and S. Speziale, Twisted geometries: A geometric parametrization of $SU(2)$ phase space, *Phys. Rev. D* **82**, 084040 (2010).
- [10] G. Long and C.-Y. Lin, Geometric parametrization of $SO(D+1)$ phase space of all dimensional loop quantum gravity, *Phys. Rev. D* **103**, 086016 (2021).
- [11] G. Long, Parametrization of holonomy-flux phase space in the Hamiltonian formulation of $SO(N)$ gauge field theory with $SO(D+1)$ loop quantum gravity as an exemplification, [arXiv:2307.05542](https://arxiv.org/abs/2307.05542).
- [12] T. Regge, General relativity without coordinates, *Nuovo Cimento* **19**, 558 (1961).
- [13] A. Ashtekar and J. Lewandowski, Quantum theory of geometry. 1: Area operators, *Classical Quantum Gravity* **14**, A55 (1997).
- [14] A. Ashtekar and J. Lewandowski, Quantum theory of geometry. 2. Volume operators, *Adv. Theor. Math. Phys.* **1**, 388 (1998).
- [15] Y. Ma, C. Soo, and J. Yang, New length operator for loop quantum gravity, *Phys. Rev. D* **81**, 124026 (2010).
- [16] E. Bianchi, The length operator in loop quantum gravity, *Nucl. Phys.* **B807**, 591 (2009).
- [17] G. Long and Y. Ma, General geometric operators in all dimensional loop quantum gravity, *Phys. Rev. D* **101**, 084032 (2020).
- [18] E. Alesci, M. Assanioussi, J. Lewandowski, and I. Mäkinen, Hamiltonian operator for loop quantum gravity coupled to a scalar field, *Phys. Rev. D* **91**, 124067 (2015).
- [19] M. Assanioussi, J. Lewandowski, and I. Mäkinen, New scalar constraint operator for loop quantum gravity, *Phys. Rev. D* **92**, 044042 (2015).
- [20] C. Zhang, S. Song, and M. Han, First-order quantum correction in coherent state expectation value of loop-quantum-gravity Hamiltonian, *Phys. Rev. D* **105**, 064008 (2022).
- [21] J. Yang and Y. Ma, New Hamiltonian constraint operator for loop quantum gravity, *Phys. Lett. B* **751**, 343 (2015).
- [22] A. Perez, The spin foam approach to quantum gravity, *Living Rev. Relativity* **16**, 3 (2013).
- [23] M. Han, Z. Huang, H. Liu, and D. Qu, Complex critical points and curved geometries in four-dimensional Lorentzian spinfoam quantum gravity, *Phys. Rev. D* **106**, 044005 (2022).
- [24] M. Han and H. Liu, Effective dynamics from coherent state path integral of full loop quantum gravity, *Phys. Rev. D* **101**, 046003 (2020).
- [25] M. Han and H. Liu, Semiclassical limit of new path integral formulation from reduced phase space loop quantum gravity, *Phys. Rev. D* **102**, 024083 (2020).
- [26] G. Long and Y. Ma, Effective dynamics of weak coupling loop quantum gravity, *Phys. Rev. D* **105**, 044043 (2022).
- [27] T. Thiemann, Gauge field theory coherent states (GCS): I. General properties, *Classical Quantum Gravity* **18**, 2025 (2001).
- [28] T. Thiemann and O. Winkler, Gauge field theory coherent states (GCS): II. Peakedness properties, *Classical Quantum Gravity* **18**, 2561 (2001).
- [29] E. Bianchi, E. Magliaro, and C. Perini, Coherent spin-networks, *Phys. Rev. D* **82**, 024012 (2010).
- [30] A. Calcinari, L. Freidel, E. Livine, and S. Speziale, Twisted geometries coherent states for loop quantum gravity, *Classical Quantum Gravity* **38**, 025004 (2020).
- [31] G. Long, C. Zhang, and X. Zhang, Superposition type coherent states in all dimensional loop quantum gravity, *Phys. Rev. D* **104**, 046014 (2021).
- [32] B. Hall, The Segal-Bargmann “coherent state” transform for compact lie groups, *J. Funct. Anal.* **122**, 103 (1994).
- [33] G. Long, X. Zhang, and C. Zhang, Twisted geometry coherent states in all dimensional loop quantum gravity: I. Construction and Peakedness properties, *Phys. Rev. D* **105**, 066021 (2022).
- [34] G. Long, Twisted geometry coherent states in all dimensional loop quantum gravity. II. Ehrenfest property, *Phys. Rev. D* **106**, 066021 (2022).
- [35] A. Ashtekar, J. Baez, A. Corichi, and K. Krasnov, Quantum geometry and black hole entropy, *Phys. Rev. Lett.* **80**, 904 (1998).
- [36] A. Ashtekar, J. C. Baez, and K. Krasnov, Quantum geometry of isolated horizons and black hole entropy, *Adv. Theor. Math. Phys.* **4**, 1 (2000).
- [37] J. Engle, A. Perez, and K. Noui, Black hole entropy and $SU(2)$ Chern-Simons theory, *Phys. Rev. Lett.* **105**, 031302 (2010).
- [38] R. K. Kaul and P. Majumdar, Quantum black hole entropy, *Phys. Lett. B* **439**, 267 (1998).
- [39] S. Song, H. Li, Y. Ma, and C. Zhang, Entropy of black holes with arbitrary shapes in loop quantum gravity, *Sci. China Phys. Mech. Astron.* **64**, 120411 (2021).
- [40] R. K. Kaul and P. Majumdar, Logarithmic correction to the Bekenstein-Hawking entropy, *Phys. Rev. Lett.* **84**, 5255 (2000).
- [41] K. A. Meissner, Black hole entropy in loop quantum gravity, *Classical Quantum Gravity* **21**, 5245 (2004).
- [42] A. Ghosh and A. Perez, Black hole entropy and isolated horizons thermodynamics, *Phys. Rev. Lett.* **107**, 241301 (2011); **108**, 169901(E) (2012).
- [43] A. Ghosh and P. Mitra, An improved lower bound on black hole entropy in the quantum geometry approach, *Phys. Lett. B* **616**, 114 (2005).
- [44] A. Ghosh and P. Mitra, Fine-grained state counting for black holes in loop quantum gravity, *Phys. Rev. Lett.* **102**, 141302 (2009).
- [45] R. Basu, R. K. Kaul, and P. Majumdar, Entropy of isolated horizons revisited, *Phys. Rev. D* **82**, 024007 (2010).
- [46] J. Engle, K. Noui, A. Perez, and D. Pranzetti, Black hole entropy from an $SU(2)$ -invariant formulation of type I isolated horizons, *Phys. Rev. D* **82**, 044050 (2010).
- [47] A. Majhi, The microcanonical entropy of quantum isolated horizon, “quantum hair” N and the Barbero–Immirzi parameter fixation, *Classical Quantum Gravity* **31**, 095002 (2014).

- [48] A. Majhi and P. Majumdar, Quantum hairs and entropy of the quantum isolated horizon from Chern-Simons theory, *Classical Quantum Gravity* **31**, 195003 (2014).
- [49] S. Song, G. Long, C. Zhang, and X. Zhang, Thermodynamics of isolated horizons in loop quantum gravity, *Phys. Rev. D* **106**, 126007 (2022).
- [50] P. Majumdar, A possible quantum gravity hint in binary black hole merger, *Phys. Lett. B* **849**, 138467 (2024).
- [51] W. Donnelly, Entanglement entropy in loop quantum gravity, *Phys. Rev. D* **77**, 104006 (2008).
- [52] A. Perez, Statistical and entanglement entropy for black holes in quantum geometry, *Phys. Rev. D* **90**, 084015 (2014); **90**, 089907(E) (2014).
- [53] A. Dasgupta, Semi-classical quantisation of space-times with apparent horizons, *Classical Quantum Gravity* **23**, 635 (2006).
- [54] W. Donnelly, Decomposition of entanglement entropy in lattice gauge theory, *Phys. Rev. D* **85**, 085004 (2012).
- [55] W. Donnelly, Entanglement entropy and nonabelian gauge symmetry, *Classical Quantum Gravity* **31**, 214003 (2014).
- [56] N. Bodendorfer, A note on entanglement entropy and quantum geometry, *Classical Quantum Gravity* **31**, 214004 (2014).
- [57] E. R. Livine, Intertwiner entanglement on spin networks, *Phys. Rev. D* **97**, 026009 (2018).
- [58] E. R. Livine and S. Speziale, A new spinfoam vertex for quantum gravity, *Phys. Rev. D* **76**, 084028 (2007).
- [59] G. Long and N. Bodendorfer, Perelomov-type coherent states of $SO(D+1)$ in all-dimensional loop quantum gravity, *Phys. Rev. D* **102**, 126004 (2020).
- [60] E. Bianchi, P. Doná, and S. Speziale, Polyhedra in loop quantum gravity, *Phys. Rev. D* **83**, 044035 (2011).
- [61] G. Long, C.-Y. Lin, and Y. Ma, Coherent intertwiner solution of simplicity constraint in all dimensional loop quantum gravity, *Phys. Rev. D* **100**, 064065 (2019).
- [62] A. M. Perelomov, *Generalized Coherent States and Their Applications*, Theoretical and Mathematical Physics (Springer, Berlin, Heidelberg, 1986).
- [63] G. Long and Y. Ma, Polytopes in all dimensional loop quantum gravity, *Eur. Phys. J. C* **82**, 41 (2022).
- [64] L. Freidel and E. R. Livine, Spin networks for noncompact groups, *J. Math. Phys. (N.Y.)* **44**, 1322 (2003).
- [65] C. Charles and E. R. Livine, The Fock space of loopy spin networks for quantum gravity, *Gen. Relativ. Gravit.* **48**, 113 (2016).
- [66] S. Deser, R. Jackiw, and G. 't Hooft, Three-dimensional Einstein gravity: Dynamics of flat space, *Ann. Phys. (N.Y.)* **152**, 220 (1984).
- [67] L. Freidel and E. R. Livine, 3D quantum gravity and effective noncommutative quantum field theory, *Phys. Rev. Lett.* **96**, 221301 (2006).
- [68] E. R. Livine and D. R. Terno, The entropic boundary law in BF theory, *Nucl. Phys.* **B806**, 715 (2009).
- [69] Q. Chen and E. R. Livine, Intertwiner entanglement excitation and holonomy operator, *Classical Quantum Gravity* **39**, 215013 (2022).
- [70] E. Bianchi, L. Hackl, and N. Yokomizo, Entanglement entropy of squeezed vacua on a lattice, *Phys. Rev. D* **92**, 085045 (2015).
- [71] C. Delcamp, B. Dittrich, and A. Riello, On entanglement entropy in non-Abelian lattice gauge theory and 3D quantum gravity, *J. High Energy Phys.* **11** (2016) 102.
- [72] B. Baytas, E. Bianchi, and N. Yokomizo, Gluing polyhedra with entanglement in loop quantum gravity, *Phys. Rev. D* **98**, 026001 (2018).